iScience

CellPress

Article

Caloric Restriction Induces MicroRNAs to Improve Mitochondrial Proteostasis

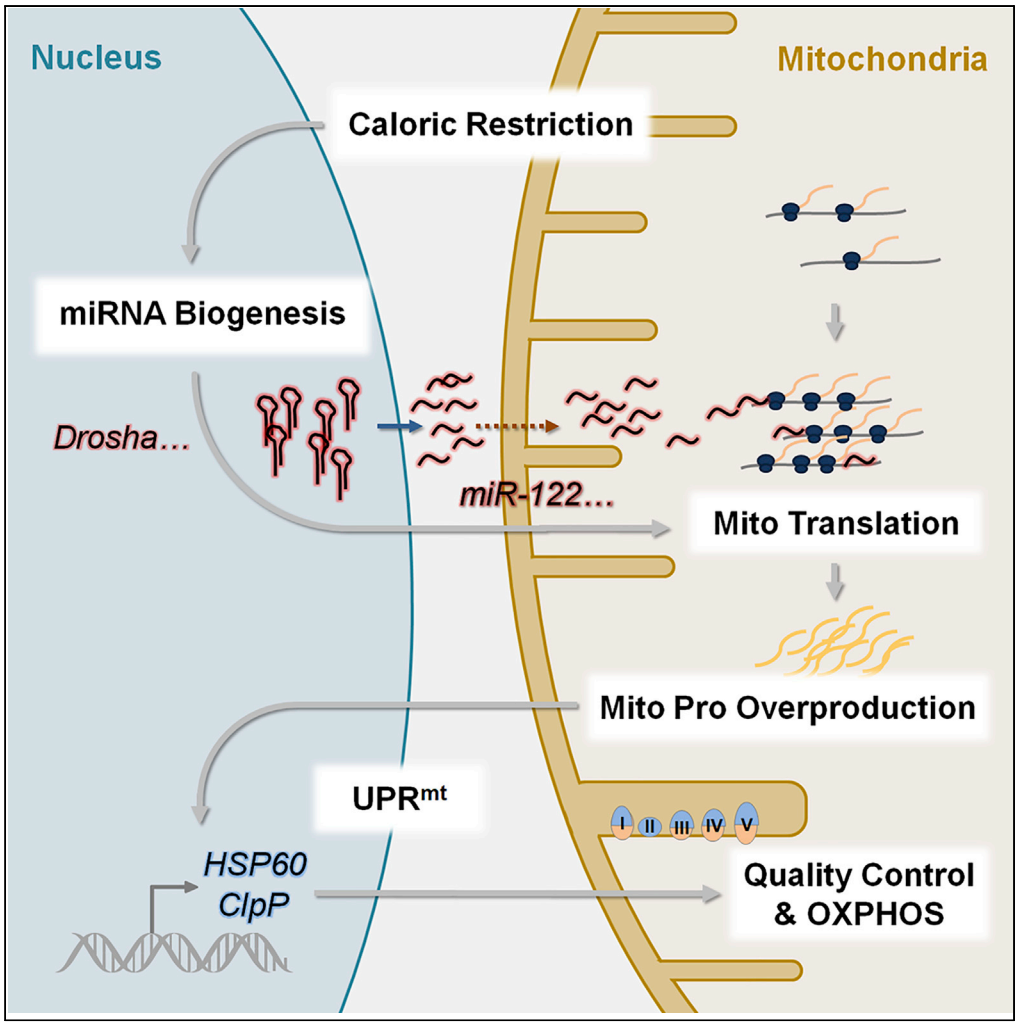

Ran Zhang, Xu Wang, Jia-Hua Qu, ..., Ping Xu, Hou-Zao Chen, De-Pei Liu

chenhouzao@ibms.cams.cn (H.-Z.C.)
liudp@pumc.edu.cn (D.-P.L.)

HIGHLIGHTS

CR increases miRNA biogenesis and the global expression of miRNAs in mitochondria

miRNAs are critical for CR-induced activation of mitochondrial translation

CR-induced miRNAs cause overproduction of mtDNA-encoded proteins and induce UPR^{mt}

Zhang et al., iScience *17*, 155–166
July 26, 2019
https://doi.org/10.1016/j.isci.2019.06.028

iScience

CellPress

Article

Caloric Restriction Induces MicroRNAs to Improve Mitochondrial Proteostasis

Ran Zhang,[1,3] Xu Wang,[1,3] Jia-Hua Qu,[1,3] Bing Liu,[1,3] Peng Zhang,[1] Tao Zhang,[2] Peng-Cheng Fan,[2] Xiao-Man Wang,[1] Guang-Yuan Xiao,[1] Ye Su,[1] Yan Xie,[1] Yue Liu,[1] Jian-Fei Pei,[1] Zhu-Qin Zhang,[1] De-Long Hao,[1] Ping Xu,[2] Hou-Zao Chen,[1,*] and De-Pei Liu[1,4,*]

SUMMARY

Both caloric restriction (CR) and mitochondrial proteostasis are linked to longevity, but how CR maintains mitochondrial proteostasis in mammals remains elusive. MicroRNAs (miRNAs) are well known for gene silencing in cytoplasm and have recently been identified in mitochondria, but knowledge regarding their influence on mitochondrial function is limited. Here, we report that CR increases miRNAs, which are required for the CR-induced activation of mitochondrial translation, in mouse liver. The ablation of miR-122, the most abundant miRNA induced by CR, or the retardation of miRNA biogenesis via Drosha knockdown significantly reduces the CR-induced activation of mitochondrial translation. Importantly, CR-induced miRNAs cause the overproduction of mtDNA-encoded proteins, which induces the mitochondrial unfolded protein response (UPR^{mt}), and consequently improves mitochondrial proteostasis and function. These findings establish a physiological role of miRNA-enhanced mitochondrial function during CR and reveal miRNAs as critical mediators of CR in inducing UPR^{mt} to improve mitochondrial proteostasis.

INTRODUCTION

Mitochondrion, a semi-autonomous organelle, encodes and locally expresses a number of subunits of the oxidative phosphorylation (OXPHOS) complexes that generate the vast majority of cellular ATP (Koopman et al., 2013). Mutations in mitochondrial DNA (mtDNA) or defects in mitochondrial translation disrupt mitochondrial proteostasis to cause serious human diseases (Boczonadi and Horvath, 2014; Kauppila et al., 2017; Park and Larsson, 2011); conversely, mild mitochondrial proteostatic stress induces the mitochondrial unfolded protein response (UPR^{mt}) to improve mitochondrial proteostasis and has been increasingly linked to longevity in *C. elegans* (Houtkooper et al., 2013). Caloric restriction (CR) without malnutrition has been proven to extend the lifespan in a wide range of organisms (Fontana and Partridge, 2015; Fontana et al., 2010). Among the myriad of CR-induced changes, mitochondrial processes, including mitochondrial proteostasis, are notably affected (Andreux et al., 2013; Cai et al., 2017; Lanza et al., 2012). However, the mechanism by which mitochondrial proteostasis is improved in mammals in the context of CR is largely unknown.

MicroRNAs (miRNAs) are evolutionarily conserved RNAs 21–22 nucleotides in length that constitute an important layer of gene regulation in eukaryotes (Chen and Rajewsky, 2007). This group of small noncoding RNAs is well known for gene silencing through either accelerating mRNA degradation or inhibiting translation in the cytoplasm (Hausser and Zavolan, 2014; Ke et al., 2003). Owing to their widespread suppressive effect at the post-transcriptional level, miRNAs reduce protein expression variation (noise) and help maintain homeostasis in diverse biological processes (Ebert and Sharp, 2012; Schmiedel et al., 2015). Recently, a few studies have suggested that CR impacts the expression levels of miRNAs in mouse serum (Dhahbi et al., 2013) and in the serum (Schneider et al., 2017) and skeletal muscle (Mercken et al., 2013) of rhesus monkeys. In addition to the canonical cytosolic localization of miRNAs, emerging evidence has identified miRNAs in mitochondria (Das et al., 2012; Jagannathan et al., 2015; Li et al., 2016; Zhang et al., 2014). Recent findings have suggested that miR-1 in skeletal muscle coordinates the myogenic program and that miR-21 in cardiac tissues lowers blood pressure by upregulating mitochondrial translation (Li et al., 2016; Zhang et al., 2014). Nevertheless, compared with the well-studied functions of miRNAs in the regulation of protein expression in the cytoplasm, the role of miRNAs in mitochondria during CR remains elusive. Therefore, it is of interest

[1]State Key Laboratory of Medical Molecular Biology, Department of Biochemistry and Molecular Biology, Institute of Basic Medical Sciences, Chinese Academy of Medical Sciences & Peking Union Medical College, Beijing 100005, P.R. China

[2]State Key Laboratory of Proteomics, National Centre for Protein Sciences Beijing, Beijing Proteome Research Centre, National Engineering Research Centre for Protein Drugs, Beijing Institute of Radiation Medicine, Beijing 102206, P.R. China

[3]These authors contributed equally

[4]Lead Contact

*Correspondence: chenhouzao@ibms.cams.cn (H.-Z.C.), liudp@pumc.edu.cn (D.-P.L.)

https://doi.org/10.1016/j.isci.2019.06.028

to investigate whether this group of regulatory RNAs is involved in the beneficial effects of CR on mitochondrial function in mammals.

In the present study, we calorie-restricted mice for 12 weeks and then performed small RNA sequencing to profile miRNA expression in mouse livers. We observed that CR increases global and mitochondrial miRNAs in mouse livers. Importantly, CR-induced miRNAs upregulate mitochondrial translation, which consequently induces UPR^{mt} to improve mitochondrial proteostasis. Our findings suggest miRNAs as a group of mediators in the regulation of mitochondrial proteostasis in response to CR.

RESULTS

CR Increases Global and Mitochondrial miRNA Levels

To investigate whether miRNAs are involved in the beneficial effects of CR in mammals, we used mice as our model organism. We fed 8-week-old male C57BL/6J mice a calorie-restricted diet for 12 weeks (20% restricted for the first week and 40% restricted for the remaining 11 week) or food *ad libitum* (AL) (Figure S1A), as previously described (Liu et al., 2016). Twelve weeks of CR significantly reduced body weight gain (Figure S1B) and reduced lipid accumulation in the liver and adipose tissues (Figures S1C and S1D). The indirect calorimetry examination results showed decreased energy expenditure and a reduced respiratory exchange rate, indicating a preference of lipids as the energy source in the CR mice (Figure S1E); we also observed that the physical activity level increased in CR mice (Figure S1F). Glucose tolerance tests suggest that CR improved glucose regulatory function in mice (Figure S1G). Consistent with a previous report (Mitchell et al., 2018), these observations suggest the successful construction of a CR mouse model, in which 12 weeks of CR significantly reprogrammed the metabolic state of the animals.

To obtain a global landscape of the miRNA profile during CR, we performed small RNA sequencing (RNA-seq) in whole liver tissues and in liver mitochondria (Figure 1A). After RNA extraction and quality control (Figures S2A and S2B), the RNA samples were spiked with *Arabidopsis thaliana* miR168a as an internal control. Analysis of the sequencing results enabled the identification of a total of 421 hepatic miRNAs in both the whole tissue and mitochondrial RNA samples (Figure S2C). As shown in the circos plot, the identified miRNAs are extensively distributed along the genome, and interestingly, the miRNAs in the whole liver tissues and in the mitochondrial samples generally increased during CR (Figure 1B). Consistently, the density plot of miRNA expression in the whole liver tissues of the CR mice exhibits a right shift from the AL mice (Figure 1C), and approximately 70% of the miRNAs were increased by CR (Figure 1D). Likewise, in the mouse liver mitochondria, the majority (~86%) of miRNAs were increased by CR (Figures 1E and 1F). After ranking the most abundant miRNAs in mouse liver and liver mitochondria, we observed that miR-122, the most abundant miRNA in the liver (Lagos-Quintana et al., 2002), accounted for the highest number of CR-induced miRNA reads in the mouse liver and liver mitochondria (Figures S2D and S2E). Particularly in the mitochondria, miR-122 increased the most during CR (Figure 1G). To confirm the CR-induced increase in miRNAs, we performed real-time PCR to examine the expression levels of the abundant miRNAs. We observed that, after normalizing against the spike-in control, the RNA levels of *GAPDH* and *β-actin* were not significantly altered, whereas the miRNAs were generally increased in the whole liver tissue samples after CR (Figure 1H). Moreover, using mouse liver mitochondrial RNA samples, we observed that, despite the lack of change in the expression of 5S rRNA, miRNAs were generally increased in the mitochondria after CR (Figure 1I). These results suggest that CR could increase miRNAs in mouse liver and liver mitochondria.

miR-122 Is Necessary for the CR-Induced Activation of Mitochondrial Translation

As miRNAs affect protein output on a large scale (Baek et al., 2008; Selbach et al., 2008), we next utilized a stable isotope labeling with amino acids in cell culture (SILAC)-based quantitative mass spectrometry (MS) approach to analyze the hepatic proteome to obtain a global insight into the effect of CR (Figures 2A and S3A–S3C). A total of 3,162 proteins were identified in samples from both the AL and CR groups (Figures S3D and S3E). Gene ontology (GO) analysis showed that the differentially expressed proteins were mostly enriched in the mitochondria (Figure 2A). We next analyzed the biological processes in which these mitochondrial proteins are involved and found that the upregulated mitochondrial proteins were most significantly clustered in the electron transport chain and metabolic pathways (Figure 2B). In contrast to the enrichment of translation among all downregulated proteins, translation was significantly upregulated among mitochondrial proteins (Figure 2C).

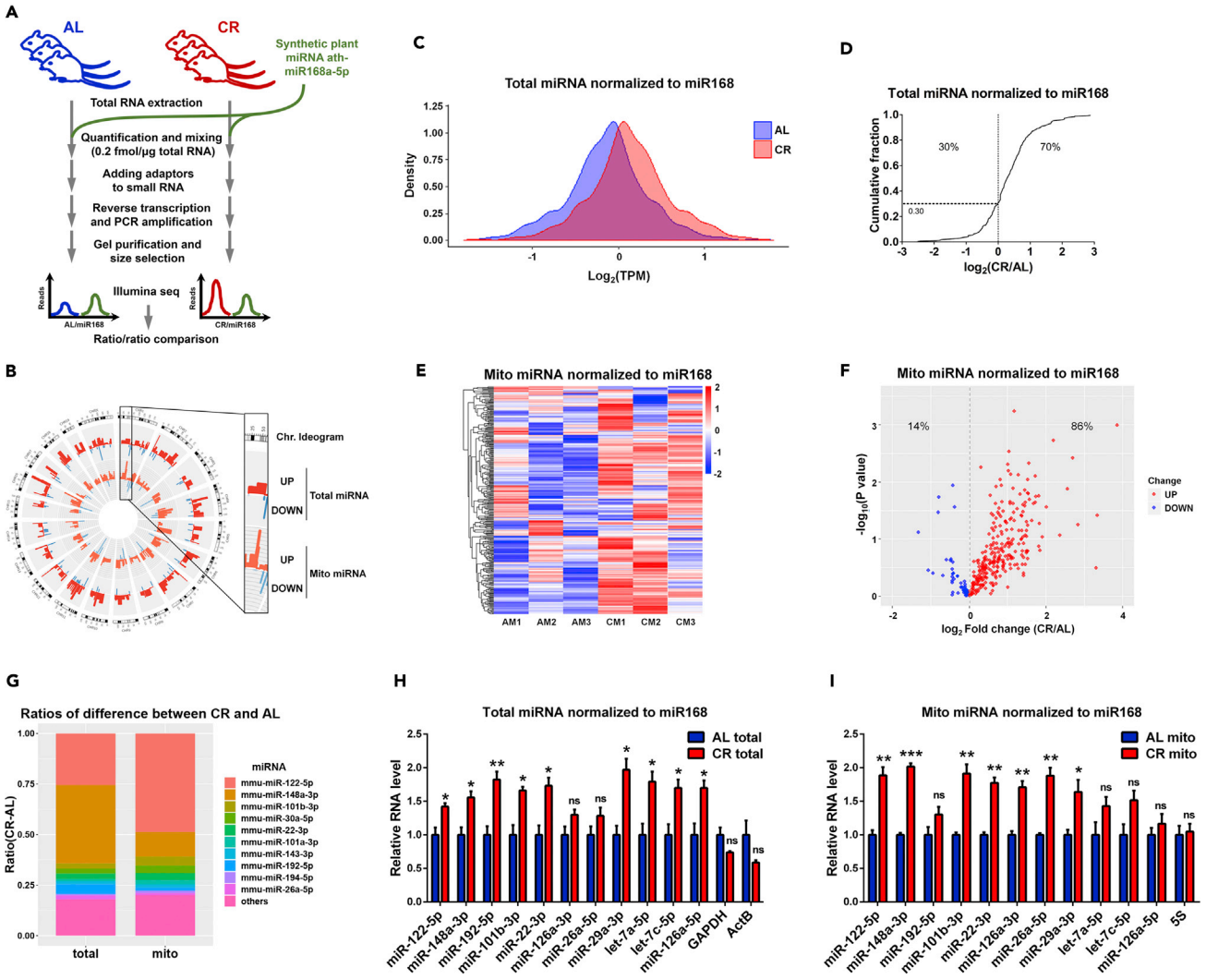

Figure 1. CR Increases Global and Mitochondrial miRNA Levels

(A) Study design for sRNA-seq of mouse livers in AL and CR groups.

(B) Circos plot of small RNA-seq dataset showing miRNAs differentially expressed in whole liver tissue (total) and in liver mitochondria (mito) in response to CR aligned to the mouse genome. The inset shows an enlarged image of chromosome 1. From the outer to the inner rings: chromosome ideogram; upregulated (red bars) and downregulated (blue bars) miRNAs in whole liver tissues; and upregulated (orange bars) and downregulated (light blue bars) miRNAs in liver mitochondria.

(C) Density plot of miRNAs identified in AL and CR mouse livers normalized to the spike-in ath-miR168a internal control.

(D) Cumulative distribution of CR-induced changes in the expression levels of miRNAs in whole-cell samples derived from mouse livers.

(E) Heatmap of commonly identified miRNAs in all samples generated by small RNA-seq. All expression levels were normalized to the exogenous ath-miR168a as an internal control. AM represents AL mitochondria, and CM represents CR mitochondria.

(F) Volcano plot of CR-induced changes in mouse liver mitochondrial miRNA expression generated by small RNA-seq.

(G) Stacked plot of the ratio of the increased Transcripts Per Million (TPM) value from AL to CR of each miRNA in mouse liver and in liver mitochondria indicated by small RNA sequencing results. miR-122-5p increased the most in the mitochondria, and miR-148a-3p increased the most in the liver during CR.

(H and I) Real-time PCR of miRNAs in whole liver tissues (H) and mouse liver mitochondria (I) in the AL and CR groups normalized to the exogenous ath-miR168a as an internal control; n = 6.

For (H and I), the data represent the mean ± SEM. p Values were obtained using unpaired t test with Welch's correction. *$p < 0.05$, **$p < 0.01$, ***$p < 0.001$, ns, not significant, compared with the respective AL group.

See also Figures S1 and S2.

Emerging evidence has suggested, in addition to the canonical gene silencing function of miRNAs in the cytoplasm (Baek et al., 2008; Selbach et al., 2008), that mitochondrial miRNAs may play a positive role in mitochondrial translation (Li et al., 2016; Zhang et al., 2014). The substantial increase in mitochondrial

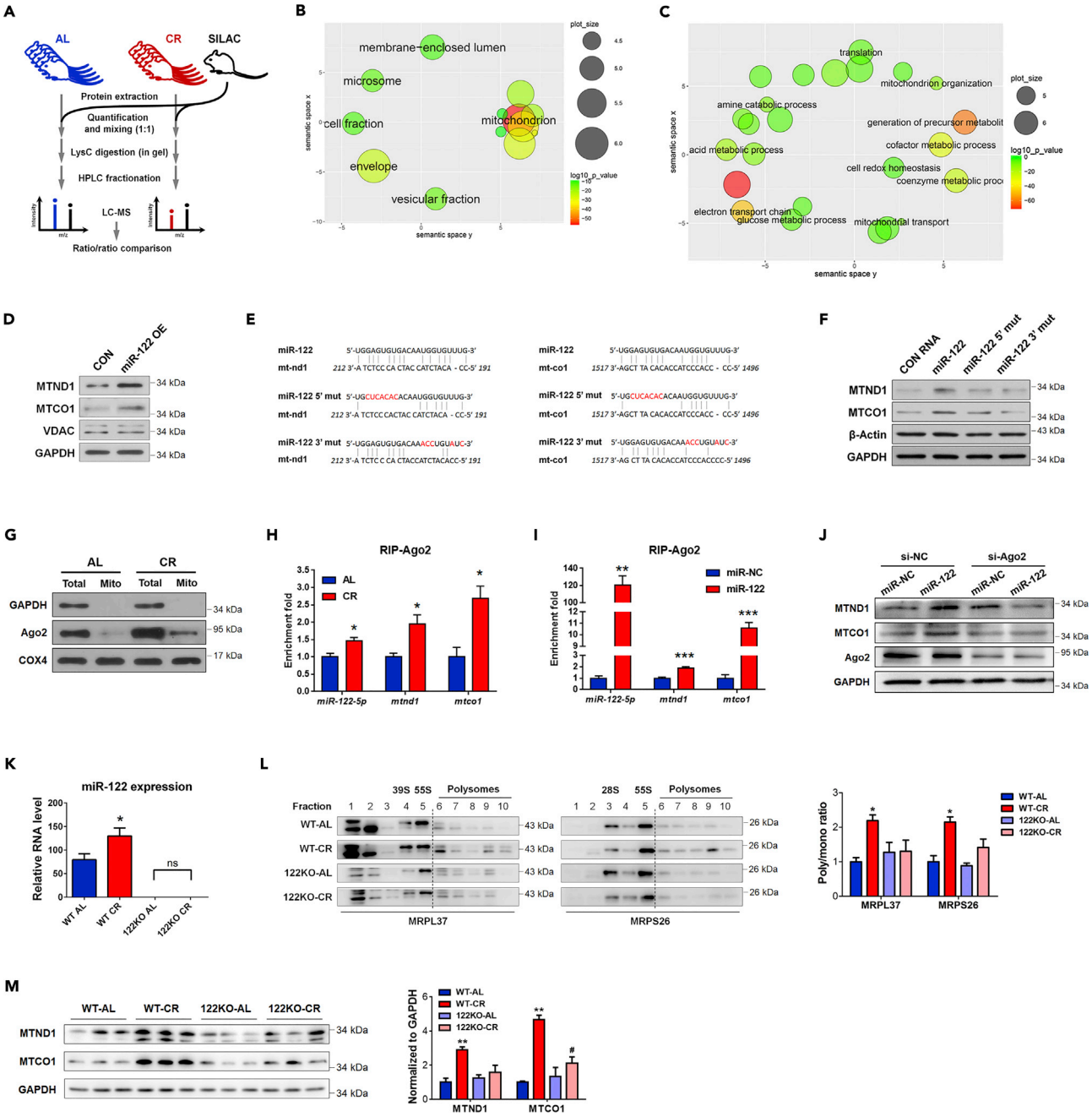

Figure 2. miR-122 Is Necessary for CR-induced Activation of Mitochondrial Translation

(A) Study design for SILAC-based relative quantitative proteomics of mouse livers in AL and CR groups.

(B) Cellular component GO analysis of differentially regulated proteins using REVIGO.

(C) Biological process GO analysis of upregulated mitochondrial proteins using REVIGO.

(D) Western blot of MTND1 and MTCO1 in Huh7 cells overexpressing miR-122.

(E) Sequences of miR-122 5′ and 3′ mutants aligned with the predicted mt-nd1 and mt-co1 target sequences.

(F) Western blot of MTND1 and MTCO1 expression in Huh7 cells upon the transfection with miR-122 and miR-122 mutants.

(G) Western blot of Ago2 in whole hepatocytes and mitochondria from the AL or CR groups.

(H and I) RNA IP of Ago2 in mouse liver mitochondria (H) or Huh7 cells (I). Bound RNA was analyzed by real-time PCR. IP efficiency was calculated relative to input. n = 3.

(J) Western blot of MTND1 and MTCO1 in Huh7 cells co-transfected with siRNA (Ago2 KD or control) and miRNA (miR-122-5p OE or control).

(K) Real-time PCR of miR-122 in livers of the miR-122 knockout (122KO) mice or the WT littermates in response to AL or CR.

Figure 2. *Continued*

(L) Mitopolysome profiling of WT and 122KO mouse liver tissues in response to AL or CR. MRPL37 and MRPS26 levels were examined. Three biological replicates from each group were pooled in equal amounts. The OD ratio of mitopolysome to mitomonosome was quantified.

(M) Western blot of MTND1 and MTCO1 in the livers of WT and 122KO mice assigned to AL or CR diet. ODs were quantified and normalized to GAPDH. The data in bar graphs represent the mean ± SEM. p Values were obtained using unpaired t test with Welch's correction.

*$p < 0.05$, **$p < 0.01$, ***$p < 0.001$, ns, not significant, compared with the AL group (H), miR-NC group (I), or WT-AL group (K)-(M). $^{\#}p < 0.05$ compared with the WT-CR group.

See also Figures S3–S5.

miRNAs in the CR mouse liver (Figure 1) and the proteome enrichment in mitochondrial translation (Figure 2C) prompted us to explore whether miRNAs are involved in the regulation of mitochondrial translation by CR. Because miR-122, the liver-specific miRNA (Chang et al., 2004; Jopling, 2012), is involved in many metabolic processes (Bian et al., 2010; Krutzfeldt et al., 2005; Yang et al., 2012) and exhibited the most abundant mitochondrial miRNA reads in the CR mouse liver (Figures S2D and S2E), we studied miR-122 as a representative miRNA in the liver mitochondria during CR.

We overexpressed the miR-122 mimic in Huh7 cells and conducted western blot analysis. We observed that miR-122 overexpression (OE) increased the protein expression levels of the mtDNA-encoded genes, including MTND1 and MTCO1 as the representative subunits of OXPHOS complexes I and IV, respectively (Koopman et al., 2013; Zhang et al., 2014) (Figure 2D). Next, we investigated whether miR-122 directly targeted *mt-nd1* and *mt-co1* mRNAs to account for their increased expression. We searched for potential miR-122-binding sites in the coding regions of *mt-nd1* and *mt-co1* using PITA (Kertesz et al., 2007) and then inserted the predicted sequences in the open reading frames of *mt-nd1* and *mt-co1* at the 3′UTR of a luciferase reporter (Figure S4A). We observed that miR-122 inhibited the luciferase activities of the reporters containing the predicted miR-122 target sites in 293T cells (Figure S4B). These data suggest that miR-122 has the capacity to directly target the predicted sites in *mt-nd1* and *mt-co1*. We further designed and synthesized an miRND1 mimic that specifically targets *mt-nd1* and an miRCO1 mimic that specifically targets *mt-co1*. After transfecting 293T cells, we observed that miRND1 robustly inhibited the luciferase activities of Luc-MTND1 and that miRCO1 suppressed the activities of Luc-MTCO1 (Figures S5A and S5B). Importantly, the western blot analysis demonstrated that, in Huh7 cells, transfection with miRND1 specifically increased the protein expression level of MTND1 (Figures S5C and S5D) and transfection with miRCO1 increased the protein expression level of MTCO1 (Figures S5C–S5E). Finally, we constructed miR-122 5′ and 3′ mutants with disrupted complementarity to the predicted binding sites at *mt-nd1* and *mt-co1* (Figure 2E) and observed that, although miR-122 increased the expression of MTND1 and MTCO1 in Huh7 cells, the mutant miR-122 mimics did not (Figure 2F). These results indicate that miR-122 increased the protein expression of MTND1 and MTCO1 through a complementary base-pairing mechanism.

In the cytoplasm, miRNAs were reported to silence gene expression by binding to Argonaute 2 (Ago2) proteins (Hock and Meister, 2008). In addition to being present in the cytoplasm, Ago2 has also been observed in the mitochondria (Zhang et al., 2014). In mouse liver mitochondria, we detected the presence of Ago2 and observed that CR increased the protein level of Ago2 in the mitochondria (Figure 2G). We next examined the binding capacity of Ago2 through RNA immunoprecipitation and quantitative PCR and observed that CR elevated the levels of miR-122 and its target mRNAs (*mtnd1* and *mtco1*) bound to the Ago2 protein in mitochondria (Figure 2H). In addition, miR-122 OE mimicked the CR effect of increasing the binding of Ago2 to *mtnd1* and *mtco1* (Figure 2I). Importantly, we co-transfected miR-122 with siRNA against Ago2 in Huh7 cells, and we observed that Ago2 KD abrogated the miR-122 OE-induced increase in the protein levels of mitochondrial-encoded genes (Figure 2J). Therefore, the increased binding of Ago2 to mitochondrial RNAs is involved in the miRNA-mediated elevation of mitochondrial translation during CR.

To further investigate the importance of endogenous miR-122 in the regulation of mitochondrial translation by CR, we used the CRISPR-Cas9 system (Wang et al., 2013) to knock out (KO) miR-122 in mice and then subjected the miR-122 KO (122KO) mice and their wild-type (WT) littermates to 12 weeks of CR. Real-time PCR revealed an increase in miR-122 as a result of CR in the WT mouse livers and the abolishment of miR-122 in the 122KO mouse livers (Figure 2K). Next, we isolated the liver mitochondria and performed mitochondrial polysome profiling to evaluate the mitochondrial translational activity. The results showed that CR increased the proportion of mitoribosomes in the polysomal fractions, demonstrating an

upregulated mitochondrial translation, but miR-122 deficiency suppressed the CR-induced upregulation (Figure 2L). Accordingly, the CR-induced increase in MTND1 and MTCO1 expression was impaired in the 122KO livers (Figure 2M). These results suggest that miR-122, the most abundant hepatic miRNA induced by CR, is critical in mediating CR-enhanced mitochondrial translation.

miRNA Biogenesis Is Required for the CR-Induced Activation of Mitochondrial Translation

In addition to increased miR-122 as a representative miRNA, the small RNA-seq results revealed that CR induced a global increase in miRNA contents in mouse livers. Therefore, we next investigated whether miRNA biogenesis, which affects the maturation of multiple miRNAs (Bartel, 2018; Treiber et al., 2018), is affected by CR and whether it is involved in the regulation of mitochondrial translation. We performed real-time PCR and observed that CR increased the RNA levels of multiple components involved in the miRNA biogenesis pathway, including *Dicer*, *Ago2*, and *exportin 5* (*Xpo5*), in mouse livers (Figure 3A). In addition, a western blot analysis showed a marked increase in these miRNA biogenesis factors, including Drosha, Dicer, and Ago2, in response to CR (Figure 3B). To study the importance of CR-induced miRNA biogenesis in the regulation of mitochondrial translation, we knocked down (KD) Drosha and Dicer, two ribonucleases required for the maturation of miRNAs, in Huh7 cells. The western blotting analysis showed that KD of either Drosha or Dicer markedly decreased the protein expression levels of the mtDNA-encoded genes MTND1 and MTCO1 (Figure 3C). Conversely, we overexpressed Drosha and Dicer in Huh7 cells and observed that, although Dicer OE did not affect MTND1 or MTCO1 expression to a measurable level, Drosha OE significantly increased MTND1 and MTCO1 expression in Huh7 cells (Figure 3D). These results suggest that Drosha might be a rate-limiting factor in the miRNA-mediated enhancement of mitochondrial translation.

Next, we knocked down Drosha (through tail vein injection of adenoviruses expressing Drosha-targeted shRNA [Adv-shDrosha]) in the C57BL/6J mouse livers after 12 weeks of CR to investigate the importance of miRNAs *in vivo* (Figure S6). The Drosha KD significantly reduced miRNAs, including miR-122 (Figure S6C). Seven days after adenovirus injection, the mouse livers were collected and the hepatic mitochondria were isolated, followed by mitochondrial polysome profiling. The results showed that CR increased the presence of mitoribosomes in the polysomal fractions from the Adv-GFP scrambled control virus-injected mice, whereas the Adv-shDrosha virus significantly prevented the CR-induced increase in mitopolysomes (Figure 3E). Accordingly, the Adv-shDrosha virus abrogated the CR-induced increase in the expression of MTND1 and MTCO1 in the liver (Figure 3F). These results suggest that augmented miRNA biogenesis is critical for the CR-induced increase in mitochondrial translation.

CR Induces the Overproduction of Mitochondrial-Encoded Proteins and UPR^{mt}

The above-mentioned results regarding the liver-specific miRNA, miR-122, and the miRNA biogenesis factor, Drosha, suggest that miRNAs are key factors in mediating the CR-induced activation of mitochondrial translation. Western blotting showed that, as a result of the upregulated mitochondrial translation, the mitochondrial-encoded proteins were overproduced (Figure 4A), raising the stoichiometric ratios of mtDNA-encoded to nDNA-encoded subunits in the same complexes (i.e., MTND1 to NDUFA9 in complex I and MTCO1 to COX4 in complex IV) (Figure 4B).

The complete structure and full function of OXPHOS complexes require precise interactions and coordination between the nDNA-encoded and mtDNA-encoded subunits (Fernandez-Vizarra et al., 2009). The moderate imbalance between mtDNA- and nDNA-encoded proteins has been shown to induce UPR^{mt} (Houtkooper et al., 2013), which responds to proteostatic stress in mitochondria to restore mitochondrial homeostasis (Haynes and Ron, 2010). Hence, we next investigated whether UPR^{mt} was induced by CR in mice. At the protein level, as suggested by our MS data (Figure 4C), although the effectors of ER UPR (UPR^{er}) and heat shock response (HSR) decreased, the UPR^{mt} effectors, including HSP60, mtHSP70, and peptidase ClpP, tended to increase during CR (Figure 4C). Western blotting confirmed a marked increase in HSP60 and ClpP expression in the CR mouse livers (Figure 4D). Consistently, real-time PCR results showed that the RNA expression levels of UPR^{mt} effectors were induced by CR at the mRNA level (Figure 4E). Next, we examined whether the overproduction of mtDNA-encoded OXPHOS subunits affects mitochondrial function. Consistent with the previous finding that CR enhances mitochondrial respiration (Lanza et al., 2012; Lopez-Lluch et al., 2006), the activities of OXPHOS complexes significantly increased in mouse livers during CR (Figure 4F). Moreover, transmission electron microscopy showed the elongation and expansion of mitochondria in the CR mouse livers, indicating an increase in the relative content of

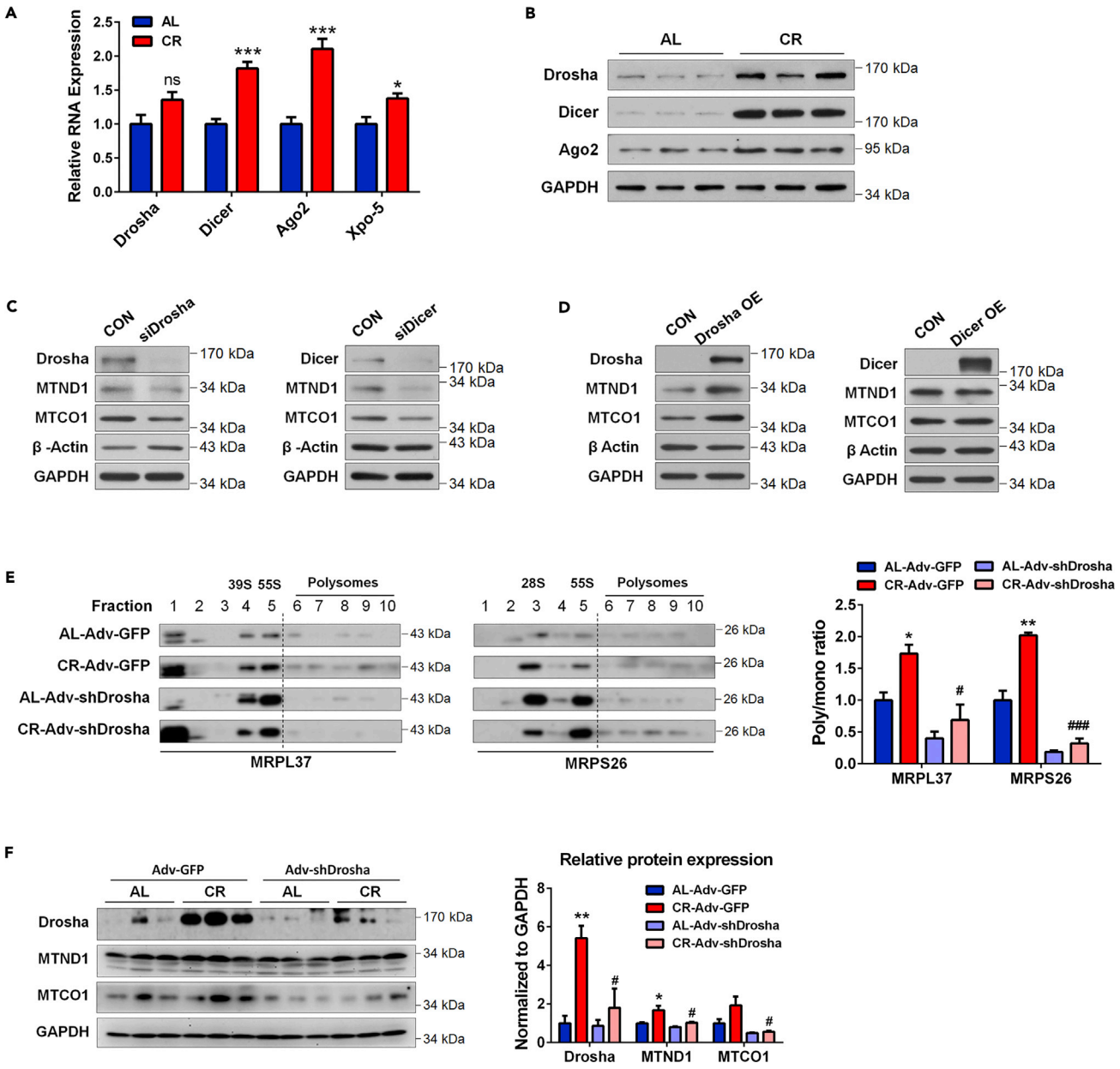

Figure 3. Drosha is the Rate-limiting Factor in CR-Induced Activation of Mitochondrial Translation

(A) Real-time PCR of miRNA biogenesis factors in mouse livers in the AL and CR groups normalized to *β-actin*; n = 6.

(B) Western blot of miRNA biogenesis factors in liver tissues from AL and CR groups.

(C and D) Western blot of MTND1 and MTCO1 in response to siRNA-mediated knockdown (KD, C) and overexpression (OE, D) of Drosha or Dicer in Huh7 cells.

(E) Mitopolysome profiling of mouse liver tissues in response to GFP control and shDrosha adenovirus infection. MRPL37 and MRPS26 levels were examined. Three biological replicates from each group were pooled in equal amounts. The OD ratio of mitopolysome to mitomonosome (55S) was quantified.

(F) Western blot of MTND1 and MTCO1 in the livers of mice in the AL and CR groups infected with GFP control or shDrosha adenovirus. ODs were quantified and normalized to GAPDH.

For A, E, and F, the data represent the mean ± SEM. p Values were obtained using unpaired t test with Welch's correction. *$p < 0.05$, **$p < 0.01$, ***$p < 0.001$, ns, not significant, compared with the AL-Adv-GFP group. $^{\#}p < 0.05$, $^{\#\#\#}p < 0.001$, compared with the CR-Adv-GFP group.

See also Figure S6.

mitochondria and improved mitochondrial morphology in response to CR (Figures 4G and 4H). Taken together, these observations support improved mitochondrial proteostasis and mitochondrial function in the mouse liver after CR.

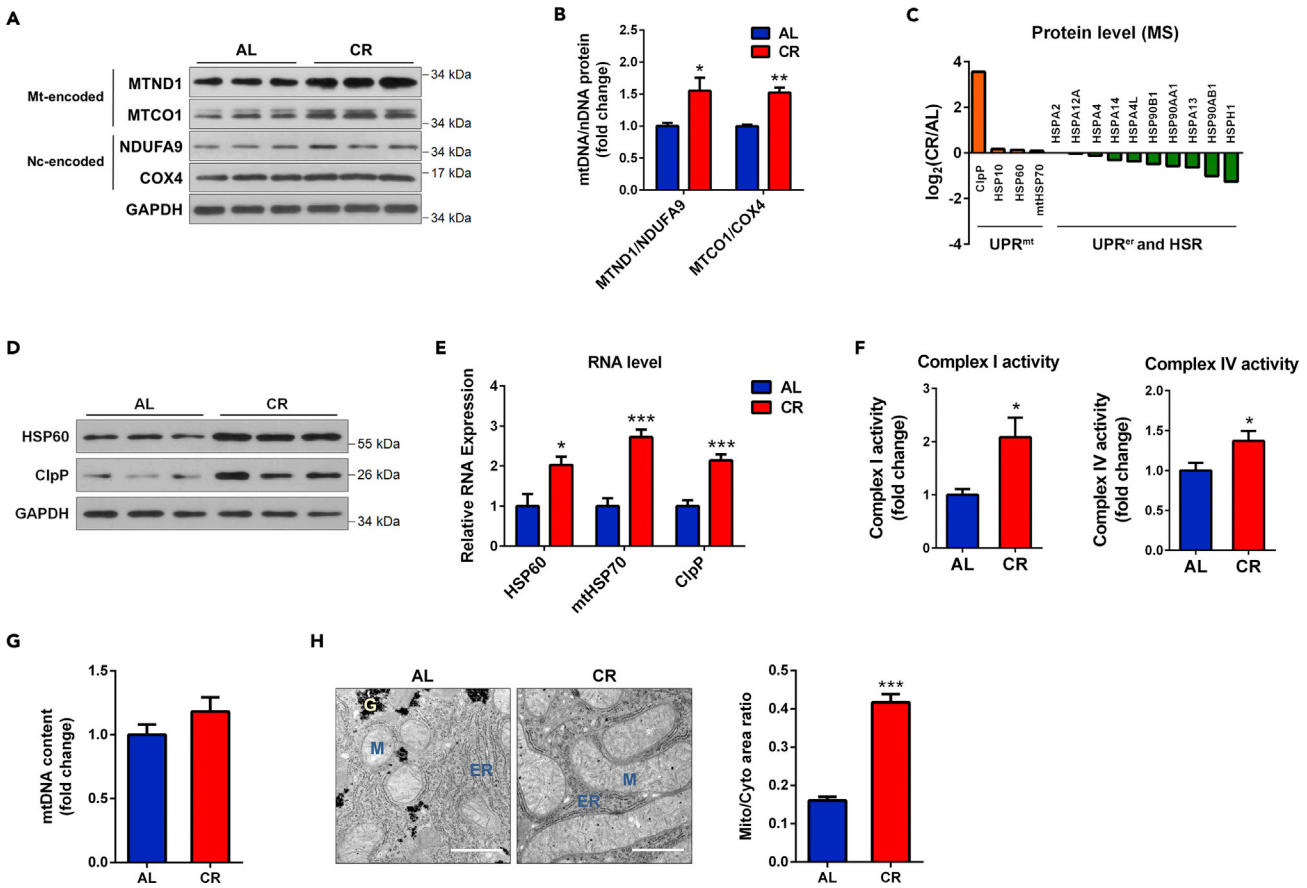

Figure 4. CR Induces the Overproduction of Mitochondrial DNA-Encoded Proteins and UPR^{mt}

(A) Western blot of the mtDNA and nDNA-encoded mitochondrial subunits in mouse livers in the AL and CR groups.

(B) OD ratios of the nDNA-encoded to mtDNA-encoded subunits of blots (A) were quantified; n = 3.

(C) Protein levels of UPR^{mt}, UPR^{er}, and heat shock response (HSR) effectors in the AL and CR groups obtained from the MS dataset.

(D) Western blot of the UPR^{mt} effectors HSP60 and ClpP in mouse livers in the AL and CR groups.

(E) Real-time PCR of the UPR^{mt} effectors in mouse livers in the AL and CR groups; n = 5.

(F) Activities of mitochondrial complexes I (left) and IV (right) in mouse livers in the AL and CR groups; n = 6.

(G) mtDNA contents in mouse livers in the AL and CR groups were examined by real-time PCR quantification of the mtDNA to nuclear genome ratios; n = 6.

(H) Representative images of mitochondria in mouse livers in the AL and CR groups obtained using a transmission electron microscope. M indicates mitochondria. ER indicates endoplasm reticulum. G indicates glycogen. Scale bars represent 2 μm. The ratio of mitochondrial to cytoplasmic area was quantified using Image-Pro Plus; n = 6.

The data in bar graphs represent the mean ± SEM. p Values were obtained using unpaired t test with Welch's correction. *p < 0.05, **p < 0.01, ***p < 0.001, compared with the corresponding AL group.

miRNAs Mediate CR-Induced UPR^{mt} and Enhancement of Mitochondrial Function

To investigate the importance of CR-induced miRNAs in the regulation of mitochondrial function, we overexpressed Drosha in Huh7 cells and examined the expression of UPR^{mt} effectors. Western blot analysis showed that Drosha OE increased ClpP expression in Huh7 cells (Figure 5A). Hence, we next investigated the involvement of miRNAs in enhancing mitochondrial activities. We observed that Drosha OE increased the activities of the mitochondrial OXPHOS complexes I and IV in transfected Huh7 cells (Figure 5B). Additionally, we overexpressed miR-122 in Huh7 cells and observed that miR-122 OE increased the expression of both HSP60 and ClpP (Figure 5C) as well as the activities of the mitochondrial OXPHOS complexes I and IV in Huh7 cells (Figure 5D). To further study the importance of endogenous miRNAs in CR-induced UPR^{mt} and enhanced mitochondrial complex activities, we examined the expression of UPR^{mt} effectors in the livers of WT and 122KO mice fed an AL or CR diet. The results showed that, although CR increased HSP60 and ClpP expression in the livers of WT littermates, the effects were lost in the livers of the 122KO mice (Figure 5E). In addition, CR significantly reinforced the activities of the mitochondrial OXPHOS

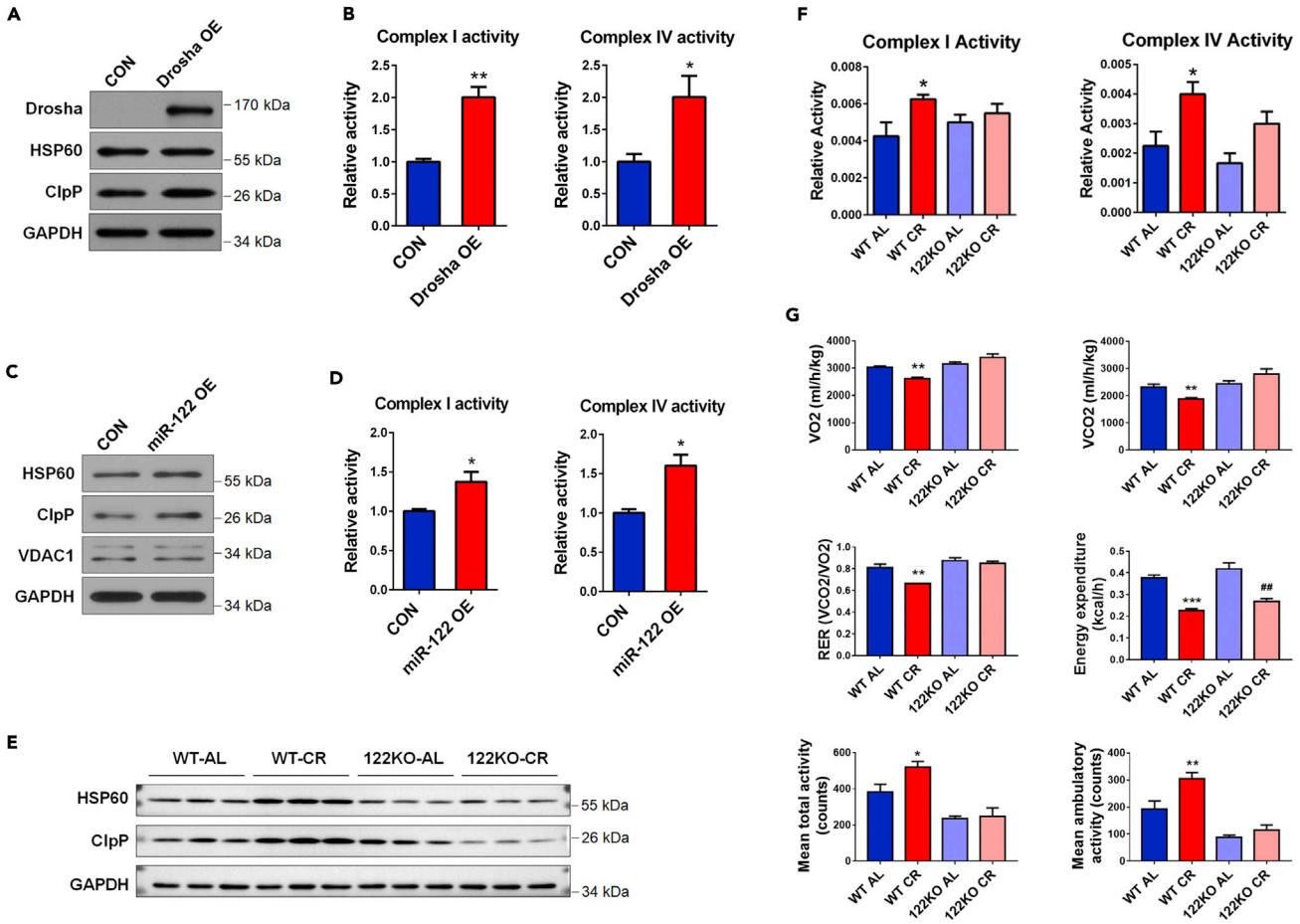

Figure 5. miRNAs Mediate CR-Induced UPR^{mt} and Enhancement of Mitochondrial Function

(A and C) Western blot of HSP60 and ClpP in Huh7 cells overexpressing Drosha (A) or miR-122 (C).

(B and D) Activities of the mitochondrial complexes I (left) and IV (right) in Huh7 cells overexpressing Drosha (B) or miR-122 (D); n = 3.

(E) Western blot of HSP60 and ClpP in the livers of WT and 122KO mice in response to AL or CR diet; n = 3.

(F) Activities of the mitochondrial complexes I (left) and IV (right) in the livers of WT and 122KO mice in response to AL or CR diet; n = 4.

(G) Indirect calorimetric examination of oxygen consumption, carbon dioxide production, energy expenditure, respiratory exchange rate (RER), and total and ambulatory activity of WT or 122KO mice in the AL and CR groups; n = 5.

The data in bar graphs represent the mean ± SEM. p Values were obtained using unpaired t test with Welch's correction. *$p < 0.05$, **$p < 0.01$, ***$p < 0.001$, compared with the corresponding control or WT-AL group. $^{\#\#}p < 0.01$, compared with the 122KO-AL group.

complexes I and IV in the WT mice but not in the 122KO mice (Figure 5F). Consistently, 122KO weakened CR-induced metabolic reprogramming, such as the improvement in the overall energy metabolism and physical activity, except for the effect on energy expenditure, providing the possibility that CR-induced miRNAs in liver exert the beneficial effects on whole body (Figure 5G). Together, CR-induced miRNAs, particularly miR-122, are important for the CR-induced UPR^{mt} and enhanced mitochondrial function.

DISCUSSION

In summary, we report that CR induced a global increase in miRNAs in a mouse model to improve mitochondrial proteostasis in mice. Specifically, at least partially by upregulating translation in the mitochondria, CR-induced miRNAs caused the overproduction of mtDNA-encoded proteins, which resulted in mild proteostatic stress in the mitochondria and consequently induced UPR^{mt} to enhance mitochondrial proteostasis and function. Moreover, we demonstrated that the ablation of miR-122, the most abundant hepatic mitochondrial miRNA, or knockdown of Drosha, a key ribonuclease for miRNA biogenesis, blunts the effect of CR on the regulation of mitochondrial translation, UPR^{mt}, and mitochondrial function.

Therefore, our study uncovered the previously unrecognized critical role of miRNAs in linking CR to improved mitochondrial proteostasis and function.

In the present study, we observed that CR increased mitochondrial miRNAs in mouse livers and that miR-122, the most abundant and liver-specific miRNA (Chang et al., 2004; Jopling, 2012), accounted for the highest number of reads that were induced in mitochondria during CR. The identification of mitochondrial miRNAs has received increasing attention. Unlike miRNAs in the cytoplasm, tissue-specific mitochondrial miRNAs have been reported to activate mitochondrial translation in the myoblasts and cardiomyocytes (Li et al., 2016; Zhang et al., 2014). In the present study, we confirmed the positive effect of miRNAs on mitochondrial protein expression in liver by observing that miR-122 increased the expression of the OXPHOS subunits MTND1 and MTCO1. Mechanistically, the positive regulation of mitochondrial-encoded genes by miR-122 appears to rely on a complementary base-pairing mechanism and the binding of Ago2 to mitochondrial targets (Figures 2 and S4). Furthermore, the observation that synthetic miRND1 and miRCO1 specifically upregulate the protein expression of their mitochondrial targets MTND1 and MTCO1, respectively (Figure S5), suggests a potentially universal mechanism by which miRNAs activate the protein expression of their mitochondrial targets.

After being transcribed, the levels of mature miRNAs are determined by the efficiency of miRNA processing (Treiber et al., 2018). A previous study reported that Dicer is downregulated in adipose tissue as mice age, thus resulting in declined miRNA processing and the decrease in multiple miRNAs, but CR can prevent the miRNA decline (Mori et al., 2012). In the present study, we found that CR upregulates several miRNA biogenesis factors in the mouse liver, among which Drosha is an important factor mediating the effect of CR (Figure 3). The knockdown or overexpression of Drosha can downregulate or upregulate the expression of mt-encoded proteins, respectively (Figures 3B and 3C). Although more detailed mechanisms related to the upregulation of mitochondrial translation by mitochondrial miRNAs remain to be examined, we demonstrated that either knockdown of Drosha or knockout of miR-122 largely reduces the effect of CR on the activation of mitochondrial translation and the improvement of mitochondrial proteostasis *in vivo*. Therefore, CR-induced miRNA biogenesis and the increased miRNA in mitochondria may play an important physiological role in the upregulation of mitochondrial translation in metabolic systems.

Because different miRNAs target different regions in the mitochondrial OXPHOS complexes, CR-induced miRNAs might collectively contribute to the redundant accumulation of mtDNA-encoded OXPHOS subunits in the mitochondria (Figure 4A). Consistently, Gomes et al. have shown that, owing to HIF-1α upregulation and TFAM downregulation, aging is associated with a specific decline in mitochondrial-encoded OXPHOS subunits, whereas CR reverses this decline by activating NAD-SIRT1 pathway (Gomes et al., 2013). Thus, CR upregulates mitochondrial proteins, particularly mtDNA-encoded OXPHOS subunits, at multiple levels. The slight perturbation of the stoichiometric ratios between mtDNA- and nDNA-derived protein subunits often induces UPR^{mt}, a retrograde pathway that induces a suite of mitochondrial chaperones and proteases (Haynes and Ron, 2010), to augment the stress resistance to improve mitochondrial proteostasis, which is regarded as a conserved longevity mechanism (Houtkooper et al., 2013). However, most previously reported interventions induce UPR^{mt} at the cost of physical functions, and these potential side effects limit their clinical application (Copeland et al., 2009; Dillin et al., 2002; Houtkooper et al., 2013; Lee et al., 2003; Redman et al., 2018; Yee et al., 2014). CR, as a physiological stimulation (Lanza et al., 2012; Lopez-Lluch et al., 2006), was reported to induce UPR^{mt} in *Caenorhabditis elegans* (Cai et al., 2017), but whether and how UPR^{mt} is induced in calorie-restricted mammals remained unclear. In the present study, we found that CR globally induced miRNAs in the mouse liver to induce UPR^{mt} accompanied by the enhancement of OXPHOS complex activities in the mouse livers and that miRNAs are required for the CR-induced improvements even in the overall metabolism and physical activity of mice. Therefore, these findings provide new evidence supporting that CR might be an effective and safe physiological strategy to induce UPR^{mt} and improve mitochondrial proteostasis for healthy aging and longevity.

Limitations of the Study

Although we observed that the blockage of miRNA biogenesis pathway (drosha) or the ablation of the most abundant hepatic miRNA (miR-122) compromises CR-induced mitochondrial translation, mitochondrial function, and metabolic reprogramming in liver, we do not exclude the possible contribution from certain cytosolic miRNAs that silence relevant targets in the cytoplasm. Therefore, a better mechanistic understanding of how miRNAs locally regulate mitochondrial translation would help dissect the importance of mitochondrial miRNAs in mediating CR's effects.

METHODS

All methods can be found in the accompanying Transparent Methods supplemental file.

SUPPLEMENTAL INFORMATION

Supplemental Information can be found online at https://doi.org/10.1016/j.isci.2019.06.028.

ACKNOWLEDGMENTS

We thank Dr. Evan D. Rosen (Beth Israel Deaconess Medical Center, Harvard Medical School) for scientific insight. This work was supported by grants from the Chinese Academy of Medical Sciences Innovation Fund for Medical Sciences (CIFMS, 2017-I2M-1-008, 2016-I2M-1-015, 2016-I2M-1-016, 2016-I2M-1-011), the National Natural Science Foundation of China (nos. 31571193, 91639304, 91849207), and the Medical Epigenetics Research Center, Chinese Academy of Medical Sciences (2017PT31035, 2018PT31015). Dr. H.Z. Chen is also supported by the Youth Top-Notch Talent Support Program and the Youth Yangtze River Scholar Program in China.

AUTHOR CONTRIBUTIONS

R.Z., J.-H.Q, and X.-M.W performed and analyzed small RNA-seq. X.W., J.-H.Q, T.Z., P.-C.F., and P.X. performed and analyzed SILAC MS. P.Z. and G.-Y.X. constructed 122KO mice. R.Z., X.W., J.-H.Q., Y.L., and D.-L.H. performed different parts of the other experiments. R.Z., X.W., J.-H.Q., B.L., Y.X., Z.-Q.Z., P.X., H.-Z.C., and D.-P.L. analyzed and discussed the results. R.Z., X.W., J.-H.Q., H.-Z.C., and D.-P.L. conceptualized and designed the study. R.Z., J.-H.Q., H.-Z.C., and D.-P.L. wrote the manuscript. H.-Z.C. and D.-P.L. acquired the funding and supervised the study.

DECLARATION OF INTERESTS

The authors declare no competing interests.

Received: March 25, 2019
Revised: May 7, 2019
Accepted: June 17, 2019
Published: July 26, 2019

REFERENCES

Andreux, P.A., Houtkooper, R.H., and Auwerx, J. (2013). Pharmacological approaches to restore mitochondrial function. Nat. Rev. Drug Discov. *12*, 465–483.

Baek, D., Villen, J., Shin, C., Camargo, F.D., Gygi, S.P., and Bartel, D.P. (2008). The impact of microRNAs on protein output. Nature *455*, 64–71.

Bartel, D.P. (2018). Metazoan MicroRNAs. Cell *173*, 20–51.

Bian, Z., Li, L.M., Tang, R., Hou, D.X., Chen, X., Zhang, C.Y., and Zen, K. (2010). Identification of mouse liver mitochondria-associated miRNAs and their potential biological functions. Cell Res. *20*, 1076–1078.

Boczonadi, V., and Horvath, R. (2014). Mitochondria: impaired mitochondrial translation in human disease. Int. J. Biochem. Cell Biol. *48*, 77–84.

Cai, H., Rasulova, M., Vandemeulebroucke, L., Meagher, L., Vlaeminck, C., Dhondt, I., and Braeckman, B.P. (2017). Life-span extension by axenic dietary restriction is independent of the mitochondrial unfolded protein response and mitohormesis in *Caenorhabditis elegans*. J. Gerontol. A Biol. Sci. Med. Sci. *72*, 1311–1318.

Chang, J., Nicolas, E., Marks, D., Sander, C., Lerro, A., Buendia, M.A., Xu, C., Mason, W.S., Moloshok, T., Bort, R., et al. (2004). miR-122, a *Mammalian* liver-specific microRNA, is processed from hcr mRNA and may downregulate the high affinity cationic amino acid transporter CAT-1. RNA Biol. *1*, 106–113.

Chen, K., and Rajewsky, N. (2007). The evolution of gene regulation by transcription factors and microRNAs. Nat. Rev. Genet. *8*, 93–103.

Copeland, J.M., Cho, J., Lo, T., Jr., Hur, J.H., Bahadorani, S., Arabyan, T., Rabie, J., Soh, J., and Walker, D.W. (2009). Extension of *Drosophila* life span by RNAi of the mitochondrial respiratory chain. Curr. Biol. *19*, 1591–1598.

Das, S., Ferlito, M., Kent, O.A., Fox-Talbot, K., Wang, R., Liu, D., Raghavachari, N., Yang, Y., Wheelan, S.J., Murphy, E., et al. (2012). Nuclear miRNA regulates the mitochondrial genome in the heart. Circ. Res. *110*, 1596–1603.

Dhahbi, J.M., Spindler, S.R., Atamna, H., Yamakawa, A., Guerrero, N., Boffelli, D., Mote, P., and Martin, D.I. (2013). Deep sequencing identifies circulating mouse miRNAs that are functionally implicated in manifestations of aging and responsive to calorie restriction. Aging (Albany NY) *5*, 130–141.

Dillin, A., Hsu, A.L., Arantes-Oliveira, N., Lehrer-Graiwer, J., Hsin, H., Fraser, A.G., Kamath, R.S., Ahringer, J., and Kenyon, C. (2002). Rates of behavior and aging specified by mitochondrial function during development. Science *298*, 2398–2401.

Ebert, M.S., and Sharp, P.A. (2012). Roles for microRNAs in conferring robustness to biological processes. Cell *149*, 515–524.

Fernandez-Vizarra, E., Tiranti, V., and Zeviani, M. (2009). Assembly of the oxidative phosphorylation system in humans: what we have learned by studying its defects. Biochim. Biophys. Acta *1793*, 200–211.

Fontana, L., and Partridge, L. (2015). Promoting health and longevity through diet: from model organisms to humans. Cell *161*, 106–118.

Fontana, L., Partridge, L., and Longo, V.D. (2010). Extending healthy life span–from yeast to humans. Science *328*, 321–326.

Gomes, A.P., Price, N.L., Ling, A.J., Moslehi, J.J., Montgomery, M.K., Rajman, L., White, J.P., Teodoro, J.S., Wrann, C.D., Hubbard, B.P., et al. (2013). Declining NAD(+) induces a pseudohypoxic state disrupting nuclear-mitochondrial communication during aging. Cell *155*, 1624–1638.

Hausser, J., and Zavolan, M. (2014). Identification and consequences of miRNA-target interactions–beyond repression of gene expression. Nat. Rev. Genet. *15*, 599–612.

Haynes, C.M., and Ron, D. (2010). The mitochondrial UPR - protecting organelle protein homeostasis. J. Cell Sci. *123*, 3849–3855.

Hock, J., and Meister, G. (2008). The argonaute protein family. Genome Biol. *9*, 210.

Houtkooper, R.H., Mouchiroud, L., Ryu, D., Moullan, N., Katsyuba, E., Knott, G., Williams, R.W., and Auwerx, J. (2013). Mitonuclear protein imbalance as a conserved longevity mechanism. Nature *497*, 451–457.

Jagannathan, R., Thapa, D., Nichols, C.E., Shepherd, D.L., Stricker, J.C., Croston, T.L., Baseler, W.A., Lewis, S.E., Martinez, I., and Hollander, J.M. (2015). Translational regulation of the mitochondrial genome following redistribution of mitochondrial microRNA in the diabetic heart. Circ. Cardiovasc. Genet. *8*, 785–802.

Jopling, C. (2012). Liver-specific microRNA-122: biogenesis and function. RNA Biol. *9*, 137–142.

Kauppila, T.E.S., Kauppila, J.H.K., and Larsson, N.G. (2017). *Mammalian* mitochondria and aging: an update. Cell Metab. *25*, 57–71.

Ke, X.S., Liu, C.M., Liu, D.P., and Liang, C.C. (2003). MicroRNAs: key participants in gene regulatory networks. Curr. Opin. Chem. Biol. *7*, 516–523.

Kertesz, M., Iovino, N., Unnerstall, U., Gaul, U., and Segal, E. (2007). The role of site accessibility in microRNA target recognition. Nat. Genet. *39*, 1278–1284.

Koopman, W.J., Distelmaier, F., Smeitink, J.A., and Willems, P.H. (2013). OXPHOS mutations and neurodegeneration. EMBO J. *32*, 9–29.

Krutzfeldt, J., Rajewsky, N., Braich, R., Rajeev, K.G., Tuschl, T., Manoharan, M., and Stoffel, M. (2005). Silencing of microRNAs in vivo with 'antagomirs'. Nature *438*, 685–689.

Lagos-Quintana, M., Rauhut, R., Yalcin, A., Meyer, J., Lendeckel, W., and Tuschl, T. (2002). Identification of tissue-specific microRNAs from mouse. Curr. Biol. *12*, 735–739.

Lanza, I.R., Zabielski, P., Klaus, K.A., Morse, D.M., Heppelmann, C.J., Bergen, H.R., 3rd, Dasari, S., Walrand, S., Short, K.R., Johnson, M.L., et al. (2012). Chronic caloric restriction preserves mitochondrial function in senescence without increasing mitochondrial biogenesis. Cell Metab. *16*, 777–788.

Lee, S.S., Lee, R.Y., Fraser, A.G., Kamath, R.S., Ahringer, J., and Ruvkun, G. (2003). A systematic RNAi screen identifies a critical role for mitochondria in *C. elegans* longevity. Nat. Genet. *33*, 40–48.

Li, H., Zhang, X., Wang, F., Zhou, L., Yin, Z., Fan, J., Nie, X., Wang, P., Fu, X.D., Chen, C., et al. (2016). MicroRNA-21 lowers blood pressure in spontaneous hypertensive rats by upregulating mitochondrial translation. Circulation *134*, 734–751.

Liu, Y., Wang, T.T., Zhang, R., Fu, W.Y., Wang, X., Wang, F., Gao, P., Ding, Y.N., Xie, Y., Hao, D.L., et al. (2016). Calorie restriction protects against experimental abdominal aortic aneurysms in mice. J. Exp. Med. *213*, 2473–2488.

Lopez-Lluch, G., Hunt, N., Jones, B., Zhu, M., Jamieson, H., Hilmer, S., Cascajo, M.V., Allard, J., Ingram, D.K., Navas, P., et al. (2006). Calorie restriction induces mitochondrial biogenesis and bioenergetic efficiency. Proc. Natl. Acad. Sci. U S A *103*, 1768–1773.

Mercken, E.M., Majounie, E., Ding, J., Guo, R., Kim, J., Bernier, M., Mattison, J., Cookson, M.R., Gorospe, M., de Cabo, R., et al. (2013). Age-associated miRNA alterations in skeletal muscle from rhesus monkeys reversed by caloric restriction. Aging *5*, 692–703.

Mitchell, S.J., Bernier, M., Mattison, J.A., Aon, M.A., Kaiser, T.A., Anson, R.M., Ikeno, Y., Anderson, R.M., Ingram, D.K., and de Cabo, R. (2018). Daily fasting improves health and survival in male mice independent of diet composition and calories. Cell Metab. *29*, 221–228.e3.

Mori, M.A., Raghavan, P., Thomou, T., Boucher, J., Robida-Stubbs, S., Macotela, Y., Russell, S.J., Kirkland, J.L., Blackwell, T.K., and Kahn, C.R. (2012). Role of microRNA processing in adipose tissue in stress defense and longevity. Cell Metab. *16*, 336–347.

Park, C.B., and Larsson, N.G. (2011). Mitochondrial DNA mutations in disease and aging. J. Cell Biol. *193*, 809–818.

Redman, L.M., Smith, S.R., Burton, J.H., Martin, C.K., Il'yasova, D., and Ravussin, E. (2018). Metabolic slowing and reduced oxidative damage with sustained caloric restriction support the rate of living and oxidative damage theories of aging. Cell Metab. *27*, 805–815.

Schmiedel, J.M., Klemm, S.L., Zheng, Y., Sahay, A., Bluthgen, N., Marks, D.S., and van Oudenaarden, A. (2015). Gene expression. MicroRNA control of protein expression noise. Science *348*, 128–132.

Schneider, A., Dhahbi, J.M., Atamna, H., Clark, J.P., Colman, R.J., and Anderson, R.M. (2017). Caloric restriction impacts plasma microRNAs in rhesus monkeys. Aging Cell *16*, 1200–1203.

Selbach, M., Schwanhausser, B., Thierfelder, N., Fang, Z., Khanin, R., and Rajewsky, N. (2008). Widespread changes in protein synthesis induced by microRNAs. Nature *455*, 58–63.

Treiber, T., Treiber, N., and Meister, G. (2018). Regulation of microRNA biogenesis and its crosstalk with other cellular pathways. Nat. Rev. Mol. Cell Biol. *20*, 5–20.

Wang, H., Yang, H., Shivalila, C.S., Dawlaty, M.M., Cheng, A.W., Zhang, F., and Jaenisch, R. (2013). One-step generation of mice carrying mutations in multiple genes by CRISPR/Cas-mediated genome engineering. Cell *153*, 910–918.

Yang, Y.M., Seo, S.Y., Kim, T.H., and Kim, S.G. (2012). Decrease of microRNA-122 causes hepatic insulin resistance by inducing protein tyrosine phosphatase 1B, which is reversed by licorice flavonoid. Hepatology *56*, 2209–2220.

Yee, C., Yang, W., and Hekimi, S. (2014). The intrinsic apoptosis pathway mediates the pro-longevity response to mitochondrial ROS in *C. elegans*. Cell *157*, 897–909.

Zhang, X., Zuo, X., Yang, B., Li, Z., Xue, Y., Zhou, Y., Huang, J., Zhao, X., Zhou, J., Yan, Y., et al. (2014). MicroRNA directly enhances mitochondrial translation during muscle differentiation. Cell *158*, 607–619.

ISCI, Volume *17*

Supplemental Information

Caloric Restriction Induces MicroRNAs to Improve Mitochondrial Proteostasis

Ran Zhang, Xu Wang, Jia-Hua Qu, Bing Liu, Peng Zhang, Tao Zhang, Peng-Cheng Fan, Xiao-Man Wang, Guang-Yuan Xiao, Ye Su, Yan Xie, Yue Liu, Jian-Fei Pei, Zhu-Qin Zhang, De-Long Hao, Ping Xu, Hou-Zao Chen, and De-Pei Liu

SUPPLEMENTAL FIGURES AND LEGENDS

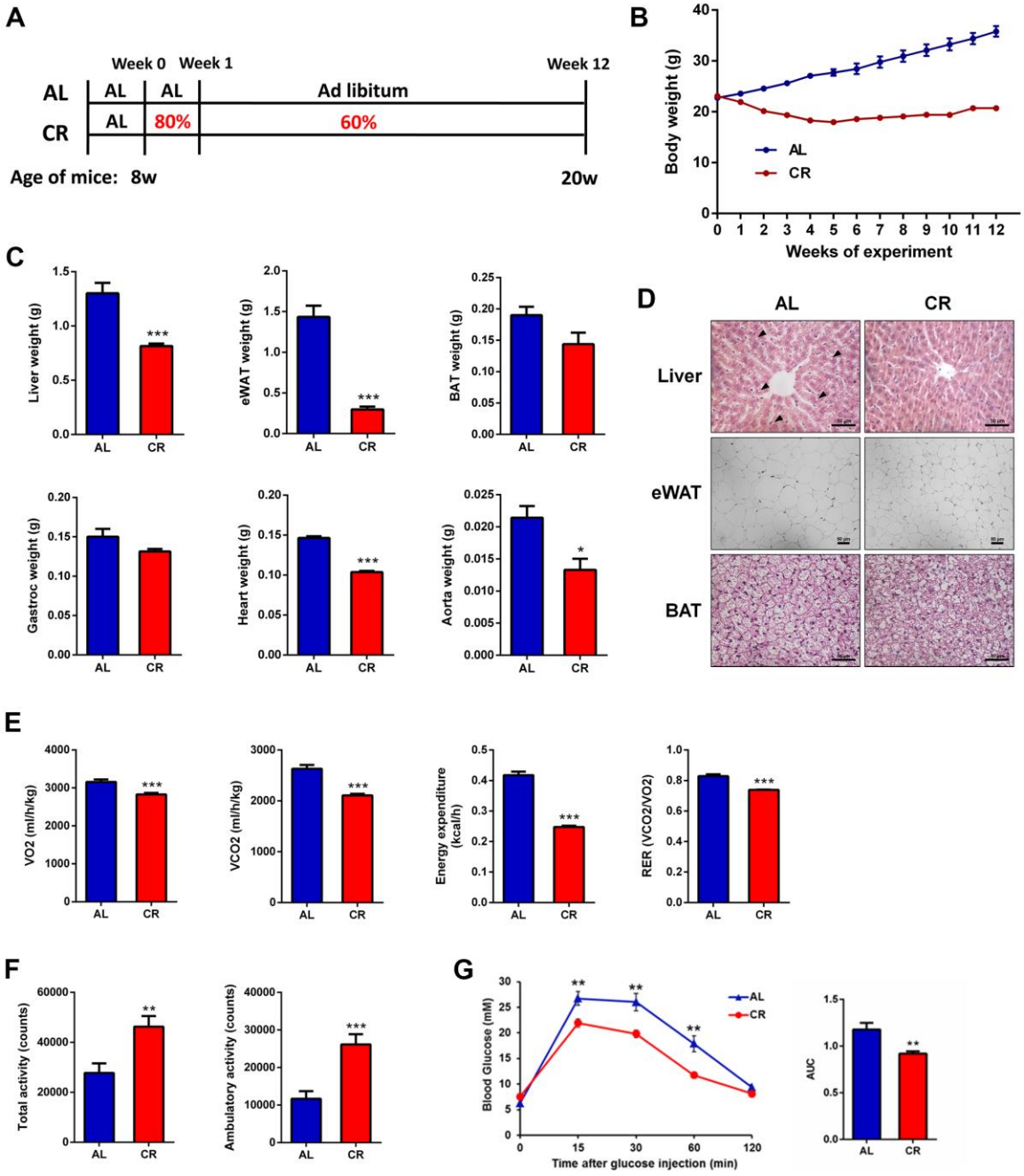

Figure S1. CR reprograms metabolism in mice, related to Figure 1.

(A) Study design for CR mouse model construction.

(B) Body weight was monitored during each week of CR; n = 10.

(C) Liver weight, epididymal white adipose tissue (eWAT) weight, brown adipose tissue (BAT) weight, gastrocnemius weight, heart weight and aorta weight examined during sacrifice; n = 10.

(D) H&E staining of liver tissues, eWAT and BAT in mice in the AL and CR groups. Black arrow heads indicate lipid droplets. Scale bars represent 50 μm.

(E), (F) Indirect calorimetric examination of oxygen consumption, carbon dioxide production, energy expenditure, respiratory exchange rate (RER) (E) and total and ambulatory activity (F) of mice in the AL and CR groups; n = 4 per group.

(G) Blood glucose levels at 0, 15, 30, 60 and 120 min after glucose injection were monitored for the intraperitoneal glucose tolerance test. The area under the curve (AUC) was calculated; n = 10 per group.

All data represent the mean ± s.e.m. For bar graphs, P values were obtained using unpaired t test with Welch's correction; for the line chart in (G), P values were obtained using repeated measures ANOVA with Tukey's multiple comparisons test. *P < 0.05, **P < 0.01, ***P < 0.001, compared with the AL group.

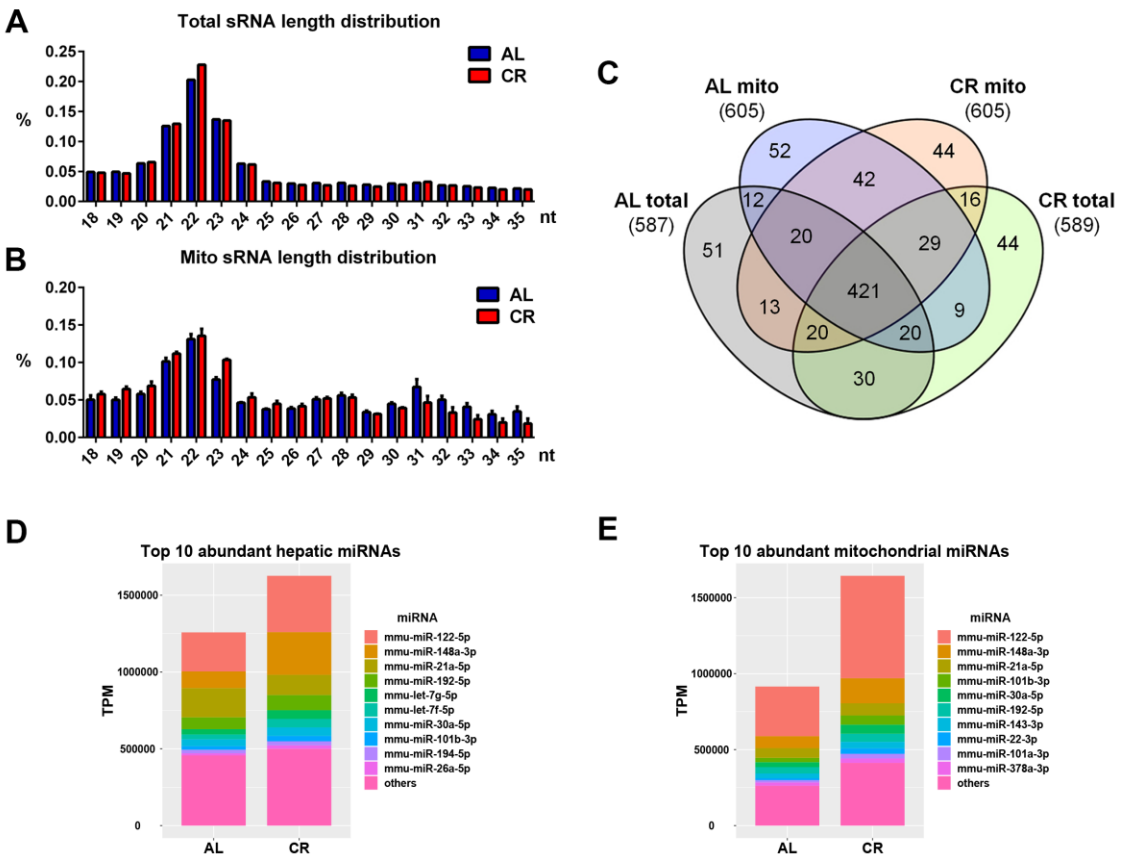

Figure S2. Sequencing of total and mitochondrial small RNAs (sRNAs) in mouse liver in response to CR, related to Figure 1.

(A), (B) Distribution of length, between 18 and 35 nt, of total sRNA (A) and mitochondrial sRNA (B) in mouse liver samples from AL and CR groups.

(C) Venn diagram of miRNAs identified in each group.

(D), (E) Stacked plots of TPM values of the top abundant miRNAs in mouse liver (D) and in liver mitochondria (E) indicated by small RNA sequencing results. miR-122-5p was the most highly abundant miRNA in the liver and mitochondria.

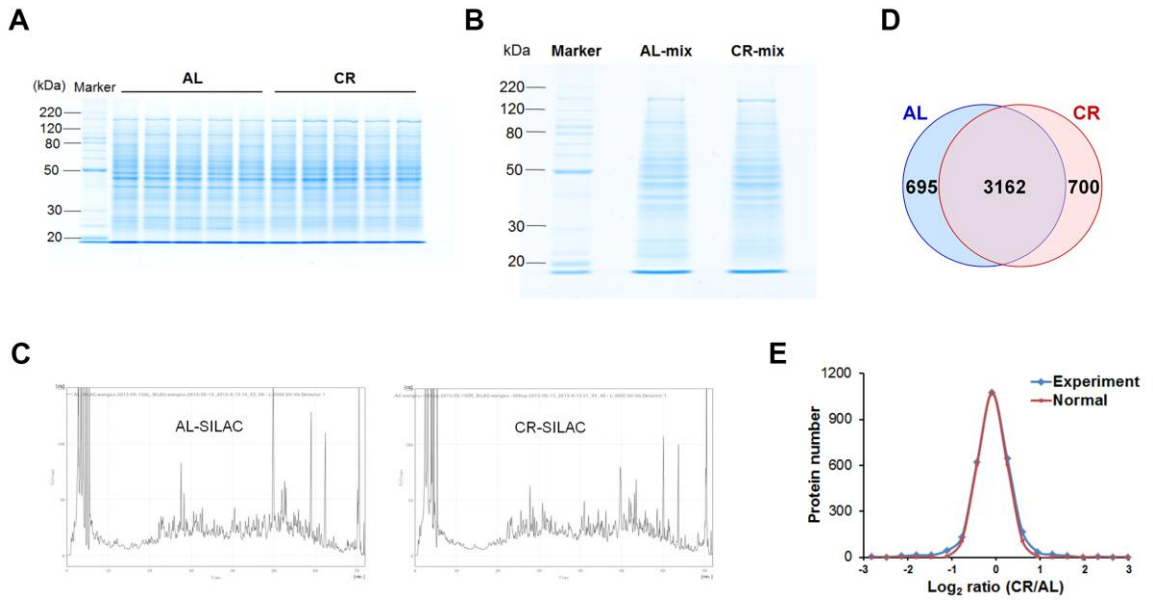

Figure S3. SILAC-based proteomics profiling of mouse livers in the AL and CR groups, related to Figure 2.

(A) Five biological replicates of liver protein samples for each group were examined by Coomassie staining.

(B) Five biological replicates from each group were pooled in equal amounts. Protein sample quality was verified by Coomassie staining.

(C) Pooled samples (SILAC sample incorporated) were fractionated using high-performance liquid chromatography (HPLC).

(D) Venn diagram of proteins identified in mouse hepatic proteomes from the AL and CR groups.

(E) Distribution of the quantified differentially expressed proteins fitted to a normal Gaussian curve.

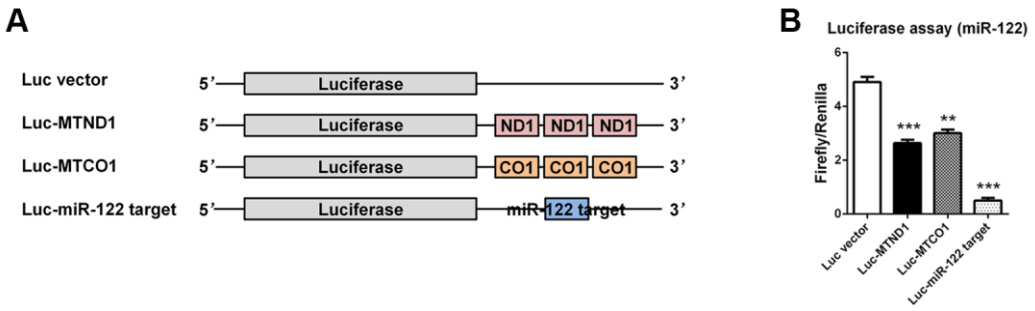

Figure S4. Dual fluorescent reporter gene assay, related to Figure 2.

(A) Schematic of luciferase vectors with predicted target sequences inserted into the 3' end of luciferase ORF.

(B) Luciferase activities using Luc-vec, Luc-MTND1, Luc-MTCO1 and Luc-miR-122 target vectors upon the transfection with miR-122 mimic in 293T cells.

All data in bar graphs represent the mean ± s.e.m. P values were obtained using unpaired t test with Welch's correction. **P < 0.01, ***P < 0.001, compared with the Luc vector group.

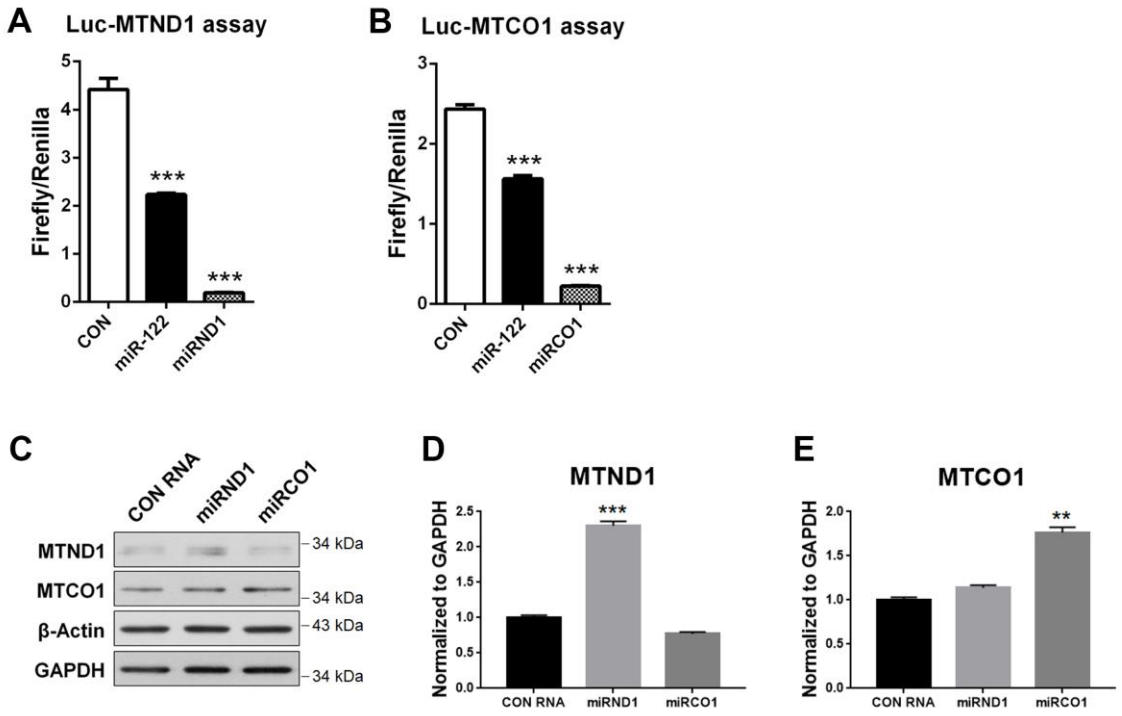

Figure S5. Synthetic miRNA mimics activate mitochondrial-encoded gene expression, related to Figure 2.

(A) Luciferase activity analysis of Luc-MTND1 in 293T cells upon the transfection with scrambled control, miR-122 or miRND1 mimic.

(B) Luciferase activity analysis of Luc-MTCO1 in 293T cells upon the transfection with scrambled control, miR-122 or miRCO1 mimic.

(C) Western blot analysis of MTND1 and MTCO1 expression in Huh7 cells upon the transfection with synthetic miRND1 and miRCO1 mimics.

(D), (E) OD values of MTND1 (D) and MTCO1 (E) in blots (C) were quantified; n = 3.

All data in bar graphs represent the mean ± s.e.m. P values were obtained using unpaired t test with Welch's correction. **P < 0.01, ***P < 0.001, compared with the corresponding scrambled control group.

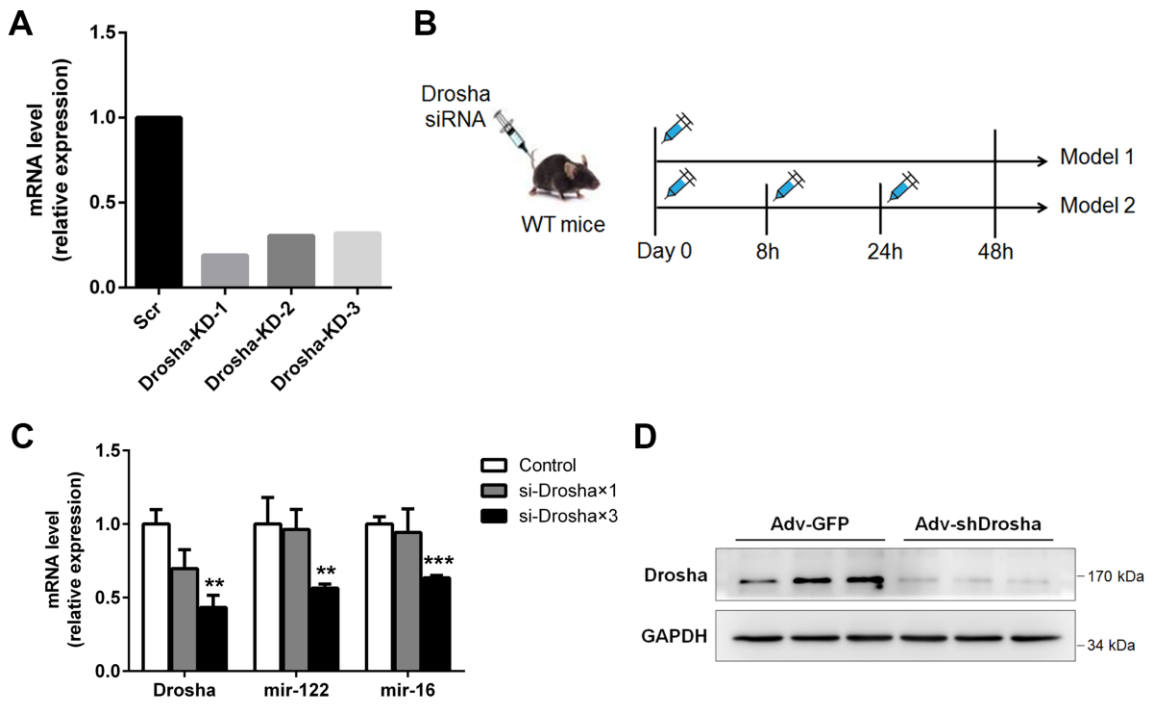

Figure S6. Verification of shDrosha adenovirus, related to Figure 3.

(A) Real-time PCR verification of Drosha KD by real-time PCR after transfection with three different Drosha siRNAs (Drosha-KD-1 to 3) in NIH3T3 cells.

(B) Hydrodynamic gene delivery of Drosha siRNA (based on the Drosha-KD-1 target sequence) through tail vein injection.

(C) Real-time PCR quantification showing that Drosha siRNA injection down-regulated hepatic miRNA levels in WT mice; n = 3.

(D) Western blotting verification of Drosha knockdown by western blotting after infection of MEFs with shDrosha adenovirus (based on the Drosha-KD-1 target sequence).

The data in bar graphs represent the mean ± s.e.m. P values were obtained using unpaired t test with Welch's correction. **P < 0.01, ***P < 0.001, compared with the scrambled (scr, control) group.

TRANSPARENT METHODS

Construction of the mouse model of caloric restriction

Eight-week-old male WT C57BL/6J mice and miR-122 knockout mice on a C57BL/6J background were housed individually and were randomly allocated into 2 groups. The AL mice were provided food *ad libitum* for 12 weeks. The CR mice were fed a 20% restricted diet for the first week and a 40% restricted diet for the remaining 11 weeks of the CR diet as previously described (Liu et al., 2016a). The compositions of the AL and CR diets were based on the chemically defined AIN-93M diet as previously described (Pugh et al., 1999). The mice were housed in a temperature-controlled environment with a 12-h light:12-h dark cycle and were allowed free access to water. The mice were weighed weekly. In the last week of the experiment, the mice underwent indirect calorimetry and an intraperitoneal glucose tolerance test (IPGTT). After the mice were sacrificed, the livers, epididymal white adipose tissue, interscapular brown adipose tissue, gastrocnemius muscles, hearts and aortic tissues were immediately harvested, weighed and analysed. All animal protocols were approved by the Animal Care and Use Committee of the Institute of Basic Medical Sciences, Chinese Academy of Medical Sciences and Peking Union Medical College.

Construction of the miR-122 KO mice

The CRISPR/Cas9 system was used to construct the miR-122 KO mice as previously described (Wang et al., 2013). The CRISPR/Cas9 vector pX330 was ordered from Addgene (Ad42230, Cambridge, MA, USA). Female C57BL/6J and BALB/c mice were used as embryo donors and foster mothers, respectively. To produce Cas9 mRNA, the T7 promoter was inserted upstream of the Cas9 open reading frame. Cas9 mRNA (200 ng/μl) and sgRNA (50 ng/μl) were injected into the cytoplasm of the fertilized eggs with well-recognized pronuclei in M2 medium (Sigma). The upstream sgRNA122 sequence was 5’-UCUGCUAAGGAAAGUCUGUC-3’; the downstream sgRNA122 sequence was 5’-ACGUCAAGUCACGCGUGGAG-3’. The injected zygotes were

cultured until the blastocyst stage for 3.5 days in KSOM with amino acids at 37℃ in a 5% CO_2 atmosphere. Thereafter, 15–25 blastocysts were transferred into the uteri of pseudopregnant BALB/c females at 2.5 days post coitum (dpc). The sequences of the primers used for genotyping were 5'-TGGAACCACTGAGGAGTCTG-3' (sense) and 5'-CATACATTACACACAATGGAGAACTC-3' (antisense).

Indirect calorimetry

After 1 day of habituation, the whole-body metabolic state of each mouse was tested for 2 days by indirect calorimetry in a CLAMS system (Columbus Instruments, America) according to the manufacturer's instructions. Light and feeding conditions were kept the same as those in the home cages. Energy expenditure (EE) and respiratory quotient (RQ) were calculated using the following equations: $EE = (0.318 \times VO_2) + (1.232 \times VCO_2)$ and $RQ = VO_2 / VCO_2$. Because of the large difference in body weight (BW) between the AL and CR mice, we compared their metabolic rates by normalizing them to the metabolic size, as reflected by the $BW^{0.75}$ of each mouse (Zhou et al., 2012).

IPGTT analysis

Prior to the IPGTT analysis, the mice were fasted overnight. Fasting blood glucose levels in blood collected via tail tip cutting were measured using a portable glucose meter (Yuwell, China). Mice were injected intraperitoneally with D-glucose (2 g/kg body weight) dissolved in saline, and blood glucose levels were measured 15, 30, 60, and 120 min after glucose injection.

Histology and electron microscopy

Mouse tissues were fixed in 4% formaldehyde (for light microscopy) or 2.5% glutaraldehyde (for electron microscopy) immediately after sacrifice. Mouse tissues were sectioned (5 μm) and then stained with haematoxylin and eosin (H&E) for light microscopy. Ultrathin (80 nm) serial

sections of mouse liver tissues were obtained for transmission electron microscopy analysis. Images were acquired using a JEOL TEM-1010 electron microscope by a single researcher who was blinded to the treatment groups.

Isolation of mitochondria and mitoplast purification

Mitochondria were isolated as previously described (Zhang et al., 2014) with slight modifications. Briefly, mouse liver tissues were homogenized in ice-cold STE buffer (250 mM sucrose, 1 mM EDTA, and 10 mM Tris-HCl, pH 7.5) with 30 to 40 strokes in a pre-chilled Dounce homogenizer and lysed on ice for 30 min. Homogenized samples were centrifuged twice at 300 g for 3 min to collect the postnuclear supernatant. Mitochondria were sedimented at 15,000 g for 15 min and washed once in the same buffer. To purify mitoplasts, the mitochondria pellet was suspended in STE buffer containing 0.5 mg/mL digitonin (Sigma, D141). After digitonin treatment on ice for 10 min, 5 volumes of STE buffer were added to the reaction, and the mitoplasts were pelleted by centrifugation at 18,000 g at 4℃ for 3 min. The mitoplast pellet was further washed 3 times with 10 volumes of STE buffer to eliminate soluble outer membrane-associated proteins.

Cell Culture and Transfection

Huh7 and 293T cells were cultured in DMEM containing 10% FBS at 37℃ in a humidified atmosphere of 5% CO2 and 95% air. Plasmids and siRNAs/miRNAs were used to transfect cells at ~70% confluence using Lipofectamine 2000 and Lipofectamine RNAiMAX (Invitrogen, 11668, 13778), respectively. pcDNA4/TO/cmycDrosha and pDESTmycDicer were ordered from Addgene (#10828, #19873). The siRNAs targeting human Drosha and Dicer are shown as follows.

	Sense	Anti-sense
si-hDrosha	GAAGCUCGAUGAAGAUUUAdTdT	UAAAUCUUCAUCGAGCUUCdTdT
si-hDicer	UGCUUGAAGCAGCUCUGGAdTdT	UCCAGAGCUGCUUCAAGCAdTdT

Small RNA-seq

RNA that was extracted from the livers of 3 mice from each group was pooled together in equal amounts to generate the total RNA samples. For the mitochondrial (mito-) RNA samples, each group contained 3 biological replicates. Before RNA extraction with TRIzol (Invitrogen, 15596018), mitochondrial samples were obtained through mitoplast purification and incubation with 10 μg/mL RNase A (Takara, 2158) on ice for 30 min to remove residual cytosolic RNA. Synthetic plant miRNAs, ath-miR168a-5p (0.2 fmol/μg total RNA) and ath-miR156a-5p (1 fmol/μg total RNA), were added to the RNA samples as exogenous internal controls. RNA integrity was examined by electrophoresis and with an Agilent 2100 bioanalyzer. Sequencing libraries were generated using NEBNext Multiplex Small RNA Library Prep Set for Illumina (NEB, E7330) following the manufacturer's recommendations, and index codes were added to attribute sequences to each sample. Small RNA libraries were sequenced with an Illumina HiSeq 2500 platform. After the removal of adapters, low quality reads and other contaminants, at least 10 M clean reads were obtained for each sample. The RNA type was analysed based on alignment with Rfam 12.0 (Nawrocki et al., 2015) and the GenBank database (Benson et al., 2013). Known miRNAs were identified by alignment with miRBase 21 (Kozomara and Griffiths-Jones, 2014). To evaluate the effect of CR on global miRNA expression, miRNA reads were normalized to exogenous plant miRNA control reads. The expression of miRNAs was visualized using Circos (Krzywinski et al., 2009). The network of representative upregulated miRNAs and their targets were generated with Cytoscape 3.4.0 (Shannon et al., 2003). The predicted targets of miRNAs were determined using miRWalk 2.0 (Dweep and Gretz, 2015). Small RNA-seq data were deposited in the GEO repository (GSE103478). Gene expression efficiencies at the post-transcriptional level were computed as the ratio of protein fold change from proteomics data to the RNA fold change from the microarray dataset.

SILAC mass spectrometry

To relatively quantify the hepatic proteome in the mice, a mouse hepatic protein sample was used as a SILAC spike-in standard, as previously described (Geiger et al., 2011). Briefly, mice were fed a 1% (Ke et al., 2003) C6-lysine SILAC diet until completely labelled F2 mice (SILAC mice) were obtained. AL and CR mouse liver tissues were lysed and sonicated, and the protein amounts were quantified. Protein samples from 5 mice in the same group were pooled together in equal amounts before being mixed with the SILAC mouse protein sample at a ratio of 1:1. The mixed protein samples were further digested by LysC protease in gel and separated with a Nano ACQUITY Ultra Performance LC (Waters) instrument. An LTQ-Orbitrap Velos was used for mass spectrometry, and Sorcerer-SEQUEST 4.0.4 (Sage-N Research) was used for protein identification. Peptides with S/N < 6 were removed. Protein expression levels were normalized to the spiked-in SILAC protein levels. Functional clustering was performed by GO analysis using DAVID 6.7, REVIGO and the ggplot2 package in R. SILAC mice were generated, and mass spectrometry was performed in Ping Xu's laboratory at the National Center for Protein Sciences in Beijing.

Mitopolysome profiling

Mitopolysome profiling was performed as previously described (Antonicka et al., 2013) with slight modifications. Mouse liver mitochondria were lysed in lysis buffer (250 mM sucrose, 100 mM KCl, 20 mM $MgCl_2$, 1% Triton X-100, 0.5 mM DTT, 0.1 mg/mL chloramphenicol, 0.5 mg/mL heparin, protease inhibitor cocktail without EDTA, and 10 mM Tris-Cl, pH 7.5) on ice for 20 min. Lysates were loaded onto a 10%–50% continuous sucrose gradient (10 mM Tris-Cl, 100 mM KCl, and 20 mM $MgCl_2$) and centrifuged at 150,000 g at 4 ℃ for 300 min using a Beckman SW41-Ti rotor. After centrifugation, 10 fractions were collected along the gradient and used for further analysis.

siRNA synthesis, adenoviral construction and tail vein injection

Three different siRNA sequences were synthesized to target mouse Drosha mRNA (shown below).

	Sense	Anti-sense
si-mDrosha #1	GGCCAACAGUCAUAGAAUAdTdT	UAUUCUAUGACUGUUGGCCdTdT
si-mDrosha #2	CCUACAAGAAAGAGUAUAAdTdT	UUAUACUCUUUCUUGUAGGdTdT
si-mDrosha #3	GGACAAGUUGAUAGGAUAUdTdT	AUAUCCUAUCAACUUGUCCdTdT

The siRNA sequence with the highest knockdown efficiency in NIH3T3 cells was used to construct adenoviruses using pHBAd-U6-GFP (Hanbio). The interference effectiveness of the siRNA sequence was verified by hydrodynamic tail vein injection as previously described (Li et al., 2011). A total of 50 μg of siRNA dissolved in 2 mL of PBS was rapidly (in 3-5 s) injected into 8- to 10-week-old male C57BL/6J mice weighing 20-25 g through the tail vein. A total of 5×10^9 PFU adenovirus in 200 μL was injected into 8- to 10-week-old male C57BL/6J mice weighing 20-25 g through the tail vein to KD Drosha in mouse livers. Mouse liver tissues were harvested 7 days after adenovirus injection.

Synthetic RNAs and miR-122 mutants

Hsa-miR-122-5p was mutated to alter the complementarity to the 5' or 3' region of the predicted target sequences on human mt-nd1 and mt-co1. The miR-122 targeted sequences on the mt-nd1 and mt-co1 gene bodies were predicted using the PITA algorithm with the lowest free energy (Kertesz et al., 2007). miR-ND1 and miR-CO1 were designed to be strictly complementary to the miR-122 targeted sequences on human mt-nd1 and mt-co1, respectively. The sequences of the synthesized miRNAs and miR-122 mutants are provided as follows.

	Sense	Anti-sense
miR-122 WT	UGGAGUGUGACAAUGGUGUUUG	AACACCAUUGUCACACUCCAUA

miR-122 5’ mutant	UGCUCACACACAAUGGUGUUUG	AACACCAUUGUGUGUGAGCAUA
miR-122 3’ mutant	UGGAGUGUGACAAACCUGUAUC	UACAGGUUUGUCACACUCCAUA
miR-ND1	UAGAGGGUGAUGGUAGAUGUAU	ACAUCUACCAUCACCCUCAUUA
miR-CO1	UCGAAUGUGUGGUAGGGUGGAU	CCACCCUACCACACAUUCUUUA
miR-22-3p	AAGCUGCCAGUUGAAGAACUGU	AGUUCUUCAACUGGCAGCUUUU
miR-148a-3p	UCAGUGCACUACAGAACUUUGU	AAAGUUCUGUAGUGCACUGAUU

Luciferase assay

The predicted has-miR-122-5p target sequences on human mt-nd1 and mt-co1 or the miR-122 reverse complementary sequence were inserted into the 3’UTR region of the pGL3-promoter luciferase vector (Promega, E1761) between the restriction sites of XbaI and FseI. Luciferase vectors were transfected into 293T cells at ~70% confluence followed by the transfection of miRNAs and miR-122 mutants 6 hr later. Cells were cultured for another 48 hr before harvesting. Luciferase activities were examined with a Dual-Luciferase Reporter Assay System (Promega, E1960) using a Modulus microplate multimode reader (Turner Biosystems). The primers used for vector construction are shown as follows.

miR-122 RC sense	CTAGTACAAACACCATTGTCACACTCCACCGG
miR-122 RC antisense	TGGAGTGTGACAATGGTGTTTGTA
Mt-ND1 sense	GCTCTAGACCACATCTACCATCACCCTCTAAACTTCCCACATCTACCATCACCCTCTACCAAT
Mt-ND1 antisense	ATTTGGCCGGCCTAGAGGGTGATGGTAGATGTGGTATTGGTAGAGGGTGATGGT
Mt-CO1 sense	GCTCTAGACCCCACCCTACCACACATTCGAAACCTTCCCCACCCTACCACACATTCGACCAAGG
Mt-CO1 antisense	ATTTGGCCGGCCTCGAATGTGTGGTAGGGTGGGGCCTTGGTCGAATGTGTGGTA

Enzyme Activity Measurement

Freshly isolated mouse livers and cultured cells were homogenized and lysed with IP lysis buffer (Beyotime Biotechnology, China, P0013). The activities of mitochondrial complex I (Abcam, ab109721) and complex IV (Abcam, ab109911) were assayed according to the manufacturers' instructions.

Relative mRNA, miRNA and mtDNA Quantifications

Total RNA was extracted using TRIzol and then reverse transcribed. Random primers (Takara, 3801) were used to reversely transcribe the RNAs. The sequences of the specific primers used for the reverse transcription of the miRNAs are shown as follows.

mmu-miR-122-5p	CTCAACTGGTGTCGTGGAGTCGGCAATTCAGTTGAGACAAACAC
mmu-miR-148a-3p	CTCAACTGGTGTCGTGGAGTCGGCAATTCAGTTGAGAACAAAGT
mmu-miR-192-5p	CTCAACTGGTGTCGTGGAGTCGGCAATTCAGTTGAGAGGCTGTC
mmu-miR-101b-3p	CTCAACTGGTGTCGTGGAGTCGGCAATTCAGTTGAGAAGCTATC
mmu-miR-22-3p	CTCAACTGGTGTCGTGGAGTCGGCAATTCAGTTGAGAACAGTTC
mmu-miR-126a-3p	CTCAACTGGTGTCGTGGAGTCGGCAATTCAGTTGAGACGCATTA
mmu-miR-26a-5p	CTCAACTGGTGTCGTGGAGTCGGCAATTCAGTTGAGAAGCCTAT
mmu-miR-29a-3p	CTCAACTGGTGTCGTGGAGTCGGCAATTCAGTTGAGATAACCGA
mmu-miR-let-7a-5p	CTCAACTGGTGTCGTGGAGTCGGCAATTCAGTTGAGAAACTATA
mmu-miR-let-7c-5p	CTCAACTGGTGTCGTGGAGTCGGCAATTCAGTTGAGAAACCATA
mmu-miR-126a-5p	CTCAACTGGTGTCGTGGAGTCGGCAATTCAGTTGAGACGCGTAC
mmu-miR-16-5p	GTCTCCTCTGGTGCAGGGTCCGAGGTATTCGCACCAGAGGAGACCG CCAA
ath-miR168a-5p	GTCGTATCCAGTGCAGGGTCCGAGGTATTCGCACTGGATACGACTT CCCG
ath-miR156a-5p	GTCGTATCCAGTGCAGGGTCCGAGGTATTCGCACTGGATACGACGT GCTC
Mouse 5S rRNA	AGCCTACAGCACCCGGTATT

Quantitative real-time PCR was performed with cDNA as a template. Target mRNA expression was calculated relative to β-actin. For mtDNA quantification, DNA was extracted using IP lysis buffer and phenol chloroform. mtDNA levels, reflected by 16S rRNA (mtDNA-encoded) PCR products, were calculated relative to 18S rRNA (nuclear DNA-encoded) PCR products using genomic DNA as a template as previously described (Liu et al., 2016b). The primer sequences for real-time PCR experiments are shown as follows.

	Sense	Anti-sense
GAPDH	CCGTAGACAAAATGGTGAAGGT	AACAATCTCCACTTTGCCACTG
β-actin	GGCTGTATTCCCCTCCATCG	CCAGTTGGTAACAATGCCATGT
18S rRNA	CGTCTGCCCTATCAACTTTCG	TGCCTTCCTTGGATGTGGTA
28S rRNA	ACGCTCATCAGACCCCAGAA	TGATTCGGCAGGTGAGTTGTT
12S rRNA	GCTCTACCTCACCATCTCTTGCTA	TTCATTGGCTACACCTTGACCTA
16S rRNA	AGGACATCCCAATGGTGTAGAAG	ATAGAAACCGACCTGGATTGCT
5S rRNA	TACGGCCATACCACCCTGA	TCCCATCCAAGTACTAACCAGG
mmu-miR-122-5p	CTGGGTGGAGTGTGACAATGGT	GGTGTCGTGGAGTCGGCAA
mmu-miR-148a-3p	CTGGGTCAGTGCACTACAGAAC	GGTGTCGTGGAGTCGGCAA
mmu-miR-192-5p	CTGGGCTGACCTATGAATTGAC	GGTGTCGTGGAGTCGGCAA
mmu-miR-101b-3p	CTGGGGTACAGTACTGTGATAG	GGTGTCGTGGAGTCGGCAA
mmu-miR-22-3p	CTGGGAAGCTGCCAGTTGAAGA	GGTGTCGTGGAGTCGGCAA
mmu-miR-126a-3p	CTGGGTCGTACCGTGAGTAATA	GGTGTCGTGGAGTCGGCAA
mmu-miR-26a-5p	CTGGGTTCAAGTAATCCAGGAT	GGTGTCGTGGAGTCGGCAA
mmu-miR-29a-3p	CTGGGTAGCACCATCTGAAATC	GGTGTCGTGGAGTCGGCAA
mmu-miR-let-7a-5p	CTGGGTGAGGTAGTAGGTTGTA	GGTGTCGTGGAGTCGGCAA
mmu-miR-let-7c-5p	CTGGGTGAGGTAGTAGGTTGTA	GGTGTCGTGGAGTCGGCAA
mmu-miR-126a-5p	CTGGGCATTATTACTTTTGGTA	GGTGTCGTGGAGTCGGCAA
mmu-miR-16-5p	CAGCCTAGCAGCACGTAAAT	GAGGTATTCGCACCAGAGGA
ath-miR168a-5p	CATATCGCTTGGTGCAGGTC	GTGCAGGGTCCGAGGT
ath-miR156a-5p	CGTGACAGAAGAGAGTGAGC	GTGCAGGGTCCGAGGT
Drosha	GGACCATCACGAAGGACACT	CACGGGTCTCTTGGTTTTGT
Dicer	ACCAAGTGATCCGTTTACGC	CAACCGTACACTGTCCATCG
Ago2	CCACCCCACTGAGTTTGACT	AACGATTGTCATCCCAAAGC

Xpo-5	GGTGGTCAACATCTGGCTTT	AGATCAGCACCCACATAGGC
ALDOA	CCTGGCTCTGGCTTTTTC	GGTGGCAGTGCTTTCCTT
SLC7A1	CATTGAAAAGACCCATTTTT	CACCTACCACTACCACCATG
GYS1	ACAGGTGGCAGCAAGAGA	ACTGGACAGGCAGGGAAT
NDRG3	CAACAAGAAGCAGCACCC	TCCAACCCCAATACCAAT
CCNG1	GCTATCTATCCTTGCGTTG	TTGGGAGGTGAGTTATTCTA
COX4I1	CGCTCGTTCTGATTTGGG	CCAGCATTCGCTTGGTCT
NDUFA9	GGACCTTCATCCCTTACCCTT	GAGATATGTATCCGCTCCACC
HSP60	TGGCTCCTCATCTCACTCGG	TCCCCAACTCTGTTCAATAATCAC
mtHSP70	GCTGTCACCAATCCAAACAATAC	ACCATTGGAGGCACGGACA
ClpP	CAGTCTGAAAGCAACAAGAAGCC	GCAGATGGGGTTCAGGATGT

Western Blotting

Primary antibodies against the following proteins were used for western blotting: RPL23 (PTG lab, 16086-1-AP), RPS27L (PTG lab, 15871-1-AP), MRPL37 (ABclonal, A4724), MRPS26 (ABclonal, A4940), VDAC1 (ABclonal, A0810), MTND1 (ABclonal, A5250), MTCO1 (Abcam, ab14705), COX4 (ABclonal, A1263), NDUFA9 (Invitrogen, 459100), Drosha (Abcam, ab12286), Dicer (Abcam, ab14601), Ago2 (Abnova, H00027161-M01), HSP60 (Abcam, ab46798), ClpP (Proteintech, HPA010649), GAPDH (CST, 5174), and β-actin (Sigma, A2228). Western blots were quantified densitometrically using Image Pro-Plus software (Media Cybernetics).

RNA Immunoprecipitation (RIP)

RNA Immunoprecipitation (RIP) was performed as previously described (Keene et al., 2006). Briefly, Huh7 cells or isolated mitochondria from mouse liver tissues were homogenized and lysed in polysome lysis buffer (100 mM KCl, 5 mM $MgCl_2$, 10 mM HEPES (pH 7.0), 0.5% NP40, 1 mM DTT, 400 μM VRC, 100 U/mL RNasin, protease inhibitor cocktail and PMSF) on ice for 20 min. Lysates were divided into Input or IP groups. Both groups were incubated with Dynabeads Protein G (Life technology, 10003D), which were coated with an antibody against

either Ago2 (Abnova, H00027161-M01) or mouse IgG (CST, #5873), diluted in NT2 buffer (150 mM NaCl, 1 mM $MgCl_2$, 0.05% NP40, and 50 mM Tris-Cl, pH 7.5), and rotated at 4℃ overnight. The beads coated with the antibody and proteins were washed with ice-cold NT2 buffer 5 times and stored in TRIzol to extract RNA. The RNA binding proteins were quantified using real-time PCR.

Data and software availability

Small RNA-seq data were deposited in the GEO repository (GSE103478). SILAC mass spectrometry data were deposited in the Mass Spectrometry Interactive Virtual Environment (MassIVE, MSV000083895).

Statistical analysis

Quantitative results are expressed as the mean ± s.e.m. The normality and the homogeneity of the variance of the data were tested. An unpaired t test with Welch's correction was used for comparisons between two groups. For comparisons among three or more groups, a one-way ANOVA with a post hoc analysis (Bonferroni test) was used for normally distributed variables, and the Kruskal-Wallis test with a post hoc analysis (Dunn's multiple comparison test) was used for variables that did not pass a normality or equal variance test. A two-way repeated measures ANOVA was used for body weight data and IPGTT data, which were repeatedly measured. All statistical analyses were carried out using GraphPad Prism 6.0 software. A P value less than 0.05 was considered statistically significant.

REFERNCES

Antonicka, H., Sasarman, F., Nishimura, T., Paupe, V., and Shoubridge, E.A. (2013). The mitochondrial RNA-binding protein GRSF1 localizes to RNA granules and is required for posttranscriptional mitochondrial gene expression. Cell Metab. 17, 386–398.

Benson, D.A., Cavanaugh, M., Clark, K., Karsch-Mizrachi, I., Lipman, D.J., Ostell, J., and Sayers, E.W. (2013). GenBank. Nucleic Acids Res. 41, D36–D42.

Dweep, H., and Gretz, N. (2015). miRWalk2.0: a comprehensive atlas of microRNA-target interactions. Nat. Methods 12, 697.

Geiger, T., Wisniewski, J.R., Cox, J., Zanivan, S., Kruger, M., Ishihama, Y., and Mann, M. (2011). Use of stable isotope labeling by amino acids in cell culture as a spike-in standard in quantitative proteomics. Nat. Protoc. 6, 147–157.

Ke, X.S., Liu, C.M., Liu, D.P., and Liang, C.C. (2003). MicroRNAs: key participants in gene regulatory networks. Curr. Opin. Chem. Biol. 7, 516–523.

Keene, J.D., Komisarow, J.M., and Friedersdorf, M.B. (2006). RIP-Chip: the isolation and identification of mRNAs, microRNAs and protein components of ribonucleoprotein complexes from cell extracts. Nat. Protoc. 1, 302–307.

Kertesz, M., Iovino, N., Unnerstall, U., Gaul, U., and Segal, E. (2007). The role of site accessibility in microRNA target recognition. Nat. Genet. 39, 1278–1284.

Kozomara, A., and Griffiths-Jones, S. (2014). miRBase: annotating high confidence microRNAs using deep sequencing data. Nucleic Acids Res. 42, D68–D73.

Krzywinski, M., Schein, J., Birol, I., Connors, J., Gascoyne, R., Horsman, D., Jones, S.J., and Marra, M.A. (2009). Circos: an information aesthetic for comparative genomics. Genome Res. 19, 1639–1645.

Li, Z.Y., Xi, Y., Zhu, W.N., Zeng, C., Zhang, Z.Q., Guo, Z.C., Hao, D.L., Liu, G., Feng, L., Chen, H.Z., et al. (2011). Positive regulation of hepatic miR-122 expression by HNF4alpha. J. Hepatol. 55, 602–611.

Liu, Y., Wang, T.T., Zhang, R., Fu, W.Y., Wang, X., Wang, F., Gao, P., Ding, Y.N., Xie, Y., Hao, D.L., et al. (2016a). Calorie restriction protects against experimental abdominal aortic aneurysms in mice. J. Exp. Med. 213, 2473–2488.

Liu, Y., Wang, T.T., Zhang, R., Fu, W.Y., Wang, X., Wang, F., Gao, P., Ding, Y.N., Xie, Y., Hao, D.L., et al. (2016b). Calorie restriction protects against experimental abdominal aortic aneurysms in mice. J Exp Med 213, 2473-2488.

Nawrocki, E.P., Burge, S.W., Bateman, A., Daub, J., Eberhardt, R.Y., Eddy, S.R., Floden, E.W., Gardner, P.P., Jones, T.A., Tate, J., et al. (2015). Rfam 12.0: updates to the RNA families database. Nucleic Acids Res. 43, D130–D137.

Pugh, T.D., Klopp, R.G., and Weindruch, R. (1999). Controlling caloric consumption: protocols for rodents and rhesus monkeys. Neurobiol. Aging 20, 157–165.

Shannon, P., Markiel, A., Ozier, O., Baliga, N.S., Wang, J.T., Ramage, D., Amin, N., Schwikowski, B., and Ideker, T. (2003). Cytoscape: a software environment for integrated models of biomolecular interaction networks. Genome Res. 13, 2498–2504.

Wang, H., Yang, H., Shivalila, C.S., Dawlaty, M.M., Cheng, A.W., Zhang, F., and Jaenisch, R. (2013). One-step generation of mice carrying mutations in multiple genes by CRISPR/Cas-mediated genome engineering. Cell 153, 910-918.

Zhang, X., Zuo, X., Yang, B., Li, Z., Xue, Y., Zhou, Y., Huang, J., Zhao, X., Zhou, J., Yan, Y., et al. (2014). MicroRNA directly enhances mitochondrial translation during muscle differentiation. Cell 158, 607-619.

Zhou, B., Yang, L., Li, S., Huang, J., Chen, H., Hou, L., Wang, J., Green, C.D., Yan, Z., Huang, X., et al. (2012). Midlife gene expressions identify modulators of aging through dietary interventions. Proc. Natl. Acad. Sci. U. S. A. 109, E1201–E1209.